Applied Spectroscopy, Available online 21 February 2022
DOI: 10.1177/00037028221085600

Physicochemical Changes in Bone Bioapatite During the Late Postmortem Interval Pre- and Post-Burning

Authors

Emese I. VÉGH[1], Nicholas MÁRQUEZ-GRANT[2] and Rick J. SCHULTING[1]

[1]Research Laboratory for Archaeology and the History of Art, School of Archaeology, University of Oxford, Dyson Perrins Building, South Parks Road, Oxford OX1 3QY, United Kingdom; email: emese.vegh@wolfson.ox.ac.uk; rick.schulting@arch.ox.ac.uk

[2]Cranfield Forensic Institute, Cranfield University, Defence Academy of the United Kingdom, College Rd, Cranfield, Wharley End, Bedford MK43 0AL, United Kingdom; email: n.marquezgrant@cranfield.ac.uk

Corresponding Author: Emese I. Végh, emese.vegh@wolfson.ox.ac.uk, Research Laboratory for Archaeology and the History of Art, University of Oxford, 1 South Parks Road, Oxford, OX1 3TG, UK

Abstract

Postmortem chemical transformation of bone bioapatite can take place during early diagenesis resulting in a more thermodynamically stable mineral phase. This paper examines the impact of a 1-year postmortem interval on unburnt and burnt bone's structural and chemical alterations. This question is of importance for the reconstruction of funerary practices involving cremation in the archaeological

record, as well as forensic anthropological investigations. Fleshed pig (*Sus scrofa*) tibiae were left exposed in a field, then collected at 14, 34, 91, 180, 365-day intervals prior to being burnt in an outdoor fire (≤750 °C bone temperature). Fresh (fleshed) tibiae acted as unburnt and burnt controls. Also included in the study were two cremated human bone fragments from Middle/Late Neolithic (ca. 3300–2500 cal BC) Ireland. Samples were analysed for major and trace elements by wavelength dispersive electron microprobe analyser (EMP-WDS) and molecular structures by Fourier Transform Infrared Spectroscopy (FTIR). Linear regression, PCA, LDA, and MANOVA were performed for statistical analysis. Results indicate that the concentrations of elements associated with extracellular fluid (K, Na, Cl) change with the postmortem interval (PMI) and survive burning. K values under 0.07 ± 0.01 wt% in inner and mid-cortical zones of burnt bones suggest that bones were not burnt immediately after death. Using this criterion, results from the archaeological samples would indicate a PMI of at least weeks to months prior to cremation. Ca, P, Fe, Al, Si, and Sr are not significantly altered with burning, and Fe, Al, Si, Sr are also unaffected by the PMI. In unburnt bones increased crystallinity and carbonate loss are detectable in <1 year, but both are obscured by burning. Structurally, the carbonate to phosphate ratio (C/P), the phosphate high temperature (PHT), and cyanamide to phosphate (CN/P) are the most useful ratios for discriminating between unburnt and burnt bones.

Keywords
cremation, electron microprobe, FTIR, taphonomy, potassium

Introduction

Thermally altered human bones occur in both forensic and archaeological contexts. Burnt bones can result from accidental fires or arson, or mask the victim's identity as well as the cause and manner of death in a homicide case. [1–3] Since antiquity, cremation has been a common funerary practice in many cultures, though there are often questions regarding the state of the corpse at the time of burning.[4–12] In several tombs and burials of Neolithic, Bronze, and Iron Age Ireland,[13–16] Scotland,[17,18] England,[19–28] and France[29,30] for example, human remains may have been excarnated before cremation, while in other cases bodies seem to have been burned soon after death.[14–16] Some of this interpretation is based on

heat-induced fracture patterns including thumbnail fractures and warping, associated with the burning of fresh bones in early studies.[31–36] However, more recent research has shown that these fractures do not depend on the presence of soft tissues, but rather on collagen content and distribution.[7,37] Recent attempts to identify bone decomposition prior to burning through histotaphonomical analysis[38] may be unreliable[39]. Identifying when burning took place after death presents a challenge, one addressed here through a study of the physicochemical changes of bones pre- and post-burning up to 1-year post-deposition.

If changes in elemental concentrations to bone are detectable after a short period of deposition/postmortem interval (PMI; in the current study 2 weeks to 1 year) and they survive burning, it can be hypothesised that it is possible to inform on the pre-burning condition, i.e., on whether bodies were fresh or partly decomposed when burnt. Although effects of diagenesis on the elemental concentration had been investigated,[40–42] no studies have examined these changes after exposure to heat. Therefore, this study aims to assess the potential of compositional and structural changes in unburnt and burnt bone to help distinguish between fresh and variably taphonomically-altered bones within a defined post-mortem interval. The results of this experiment are compared to the chemical composition of archaeological (Neolithic) cremated bones. Our hypothesis based on previous studies (e.g.[41,42]) is that these changes can occur weeks following deposition by the loss of endogenous elements in vivo and from the uptake of exogenous elements from the environment. We further hypothesise that these changes will be observed in the burnt bones since inorganic mass loss is negligible in bones burnt at up to 900°C.[43]

1.1 Taphonomic Alterations to the Elemental Concentration and Structure of Bone

Bone is a composite material consisting of ~55-70 wt% mineral, ~20-35 wt% organic carbon, and ~10-15% water.[44–46] Hydroxylapatite [HAp, $Ca_{10}(PO_4)_6(OH)_2$] is the basis of all biologically formed apatite, while bioapatite [$(Ca,Mg,Na)_{10-x}[(PO_4)_{6-x}(CO_3)_x](OH)_{2-x}$] is a carbonate-containing variety of HAp, which forms the inorganic component of bone.[45,47,48] Bioapatite is chemically more complex than HAp; it is non-stoichiometric, and can incorporate a wide variety of elements into its structure.[45,48–50]

The chemical profile of bone (Suppl. 1) results from the combination of the pre-mortem (e.g., diet, inhalation) and postmortem (e.g., degradation, soil) incorporation and release of elements. However, it is modified by taphonomic (post-mortem) factors, which can be natural (e.g., weathering, mineral replacement, microbial attack) or anthropogenically-induced (e.g., inhumation, sub-aerial exposure, disarticulation and defleshing, burning, etc.).[51,52] Early decomposition includes the hydrolysis of collagen, and the first biological, chemical, and structural changes to bioapatite.[53–56] Bioerosion causes increased surface areas which either encourages mineral dissolution or enhances the movement of ions and substitutions, eventually leading to a more thermodynamically stable mineral phase.[57] Organic loss has been associated with increased ion transport[55,57] due to the open pore spaces between the mineral phase, facilitating the movement of fluids, microorganisms, and dissolved ions,[54] unless pore spaces are blocked by ingress of trace elements from the environment.[58] Fossils, the resulting mineral phase from late diagenesis, have a wide variety of substitutions, but most commonly have F- and Ca-enriched apatite phases,[53,54,59] or CO_3^{2-} loss.[60] An experiment in which modern bones were exposed for up to 30 years on soil surfaces in Kenya showed that crystal sizes increase in number and size with time.[61]

Bone composition is susceptible to changes as soon as bone is exposed to the environment, which has been documented in unburnt modern,[41,42,62] archaeological,[63–65] and fossil bone,[57] but regarded as negligible.[66] Bioapatite can accommodate various substitutions at every site of the crystal lattice, which makes it one of the most diverse minerals.[41,67] Cations (metals) substitute for Ca(1) and Ca(2),[68] while anions for phosphates, carbonates, and hydroxyls. Trace elemental uptake due to ion exchange can occur after one week, while after a year a more thermodynamically stable mineralogical phase shift to F- and Fe-enriched apatite phases can be seen.[41] Non-uniform, non-linear increases (Mn, Fe, Ca, F) and decreases (Cl, Na) were also seen in bone buried >1 year. However, the calcium to phosphate ratio (Ca/P) remains constant during putrefaction,[69,70] while a decrease of carbonate to phosphate (C/P) has been identified after burial for 1 year. The latter is due to either carbonate loss (A and B), increased phosphate content, or the loss of organic material in bone.[41]

Much of the work on trace element uptake into bone has revolved around rare earth elements (REE) and uranium,[71–73] which are taken up by bioapatite over $10^3 – 10^6$ years post-mortem.[72] In modern bone, Ca, P (from bioapatite), Fe, Na, K (associated with bodily fluids), F, Mg, Al, Si, Cl, and Mn (associated with trace elements from soil) are usually studied. Fe, Al, and Mn are often abundant in weathered soils but are less likely to enter into solution.[74] If this does occur, Al and Mn do not only affect the outermost layers of bone, but are measurable as contaminants in the mid-cortical region in archaeological bone.[75] Fe is stored in vivo in blood, bodily organs,[42,76] with a minuscule amount being surface-bound in bone.[69,76] The decrease of Na and K has been linked to the dehydration of bone during decomposition.[42] Mg is surface-bound in bioapatite, and although it has been shown not to be much affected by diagenesis, very small amounts can be incorporated into the bioapatite lattice.[42] In buried bone cations diffuse inward toward the pores from the outer cortex.[73] Adsorption will cease once equilibrium is reached with the surrounding pore waters,[77] also evidenced by the slowing and halting of trace element leaching during fossilisation.[78] The rate of approaching equilibrium with pore waters is dependent on the element concentration, mobility in the environment, and the adsorption coefficient (i.e. a constant relating to the speed a molecule will bind to the surface of bioapatite at defined conditions).[73,77]

1.2 Heat Changes to the Physicochemical Structure of Bone

Generally, heat-induced changes in bone go through the following stages: (1) dehydration of the bone with the breakage of hydroxyl bonds and water removal; (2) organic component (lipids and proteins) decomposition around 400-500°C; (3) inversion, marked by carbonate loss (CO_3^{2-} disappears completely at ~ 700°C); and (4) fusion of the crystals (>700°C) when the crystallites grow in size and OH^- and PO_4^{2-} rearranges within the pores which are now vacant of organics and water.[37,79]

Many studies have investigated the elemental compositional changes of burnt bone in archaeological and experimental contexts,[4,49,63,71,80–84] and for biomaterials research (e.g. [85–90]). During the burning process, bone is susceptible to chemical substitutions.[91] Although in theory, most inorganic elements in bone should not change at temperatures possible to reach in an outdoor fire, the inorganic

mass loss has been shown to fluctuate around 2.8 wt% independent from temperature during heating up to 900°C.[43] Various heat-induced elemental changes have been documented (Suppl. 2.).

The main structural changes observed include the reordering of phosphate, the decrease/loss of carbonate, and increased crystallinity,[4,43,86,92–94] which start to occur at 600/700°C.[43,93,95] Extensions to the α-lattice and changes to the c-lattice parameters are accompanied by the release of lattice carbonate and possibly water, which results in an increase in crystal size and crystallinity.[96] At temperatures around 730°C, a new phase of beta-tricalcium-phosphate (β-TCP) appears in bioapatite, which remains stable at high temperatures.[97] The appearance of β-TCP signals the thermal decomposition of the apatite phase, which happens due to non-stoichiometric substitutions/P ratio (i.e. <1.67).[97,98] Another secondary phase by-product is CaO, which appears at >700°C [99] is due to the thermal decomposition of $CaCO_3$.[100]

As regards diagenetic processes, most research has investigated chemical changes to bone post-burning and after deposition,[63,81] which was thought to be similar in cremated bone as in unburnt bone in earlier research.[71,81] However, these studies were observational with no controls, [71] and only referring to calcium.[81] Bioapatite is less reactive post-deposition in an archaeological timescale[61,101] and especially after burning because the crystals transform into a more stable thermodynamic phase;[8] thus the inorganic structure seems to remain stable post-burning. The amount of organic material in bone prior to burning appears to affect thermal decomposition as traced through OH^-, carbonate (type A and B), β-TCP, tetracalcium phosphate (TetCP), loss of CO_2 and water content,[102] and presence of cyanamide.[8]

2. Materials and Methods

The material and experimental protocol employed here follows that of a parallel study,[39] which examined the histotaphonomic features in unburnt and burnt bones to inform on the PMI. Fleshed pig (*Sus scrofa domesticus)* tibiae (N=22) were allowed to decay exposed within a cage for 14 (N=5), 34 (N=5), 91 (N=5), 180 (N=5), and 365 (N=2) days prior to burning on an outdoor fire in Wytham Woods, Oxfordshire, UK. Fresh pig tibiae (N=10) served as controls throughout the study, without being exposed. Over time the exposed bones became partially submerged in soil and vegetation; however,

experimental studies have found no significant differences in elemental concentrations in buried and surface-exposed bones.[42]

Wytham Woods is located in a temperate climate with annual precipitation averaging 717 mm and mean winter and summer temperatures of 1.6°C and 20.3°C, respectively. Soil pH ranges widely from 3 to 7.[103] Bones were burnt on an outdoor fire, which was executed in the same manner with each event lasting from 2.5-3 hours until the bones were deemed to be fully calcined based on their appearance. A thermocouple was used to directly monitor bone temperature, with a mean of 553°C and a recorded maximum of 751°C.[39]

Bone samples were taken from diaphyses before and after burning to maintain consistency with other studies of elemental concentration.[42,66,104] The unburnt samples were defatted in a 2:1 chloroform:methanol mixture. The composition and atomic-level structure of the bones were analysed from: (1) polished resin blocks using wavelength-dispersive X-ray spectroscopy (WDS) on an electron microprobe (EMP); and (2) powders using Fourier Transform Infrared Spectroscopy (FTIR) in attenuated total reflectance (ATR) mode. EMP-WDS allows spatially resolved analysis of a single bone. This approach is essential, since the outer layer of the bone may have a different distribution of elements than the mid- or inner cortical bone adjacent to the medullary cavity (cf. [63]). FTIR has been used previously to determine bone composition (organic and inorganic) and bone structure, such as the infrared splitting factor (IRSF), which provides insights into bone crystallinity (e.g. [8,41]).

Additionally, two cremated human bone fragments from burials 1 and 7 at a Middle/Late Neolithic (ca. 3300–2500 cal BC) stone circle in Kiltierney, Co. Fermanagh, Northern Ireland,[105] were included. The fragments presented thumbnail fractures, suggestive of high bone collagen content at the time of burning.[7] They were analysed with EMP, to compare their bone chemistry to the experimental results.

2.1 Fourier Transform Infrared Spectroscopy (FTIR)

FTIR was used to retrieve structural and molecular information from the unburnt and burnt bones. This has been frequently used to investigate both the diagenetic pathways in osseous material,[106–

[111] to differentiate between heated bone at low, medium, and high temperatures,[112,113] and to characterise modern and archaeological burnt bone.[8,114] ATR was chosen instead of KBr discs, as it has been shown to provide more reliable measurements and fewer chemical modifications.[108,112,115–117]

The powdered pre- and post-burnt samples were measured with a Cary 600 series FTIR spectrometer 5.3 (Agilent Technologies, Santa Clara, California, USA). A diamond crystal accessory was utilised with an operational range of 30000 to 200 cm^{-1}. Resolution Pro FTIR software (Agilent Technologies, Santa Clara, California, USA) was used for automatic software correction and for generating the backgrounds and the raw data for each sample. After the spectrometer was aligned, a resolution of 4 cm^{-1} was chosen. Sixty-four scans were taken of each sample with scan range set between 4000 and 400 cm^{-1}, which represents mid-IR spectrum analysis. The background was measured after at least every second sample. Before the sample was placed on the accessory, the live spectrum was monitored to ensure no background noise. Baseline corrections were made at around 450, 800, 900, and 1200 cm^{-1}. The calculated ratios included those from the literature (Suppl. 3) and the presence of β-TCP was noted when present as a peak at 1123 cm^{-1} and as a shoulder at 547 cm^{-1}.[118] Presence of β-TCP implies that burnt bone reached >700℃. If this β-TCP peak is present at 1123 cm^{-1}, IRSF loses its usefulness in estimating crystallinity. It was also suggested that the presence of this peak might be associated with Mg substitution for Ca in the bone.[118] Type A carbonates (~1540 cm^{-1}) were not evaluated in unburnt bone, because its peak overlaps with amide II.[119] However, it was included in the burnt bone spectra evaluations, because organics were removed by heating. The peak heights were evaluated by observing the maximum height from the data at around the associated absorbance using Jupyter notebook in Python programming language. If a slight frequency shift was present (±5 cm^{-1}), the maximum height between this interval was recorded for the ratio calculations and the extent of shift noted.

2.2 Electron Microprobe Analysis (EMPA)

A total of 58 unburnt and burnt bone fragments were embedded undecalcified into epoxy cold mounting resin and a catalyst (Spectrographic Ltd., Leeds, UK) and placed under vacuum in a desiccator

to ensure diffusion of the resin into bone pores. Mounted blocks were then ground with carbon papers of progressively finer grit size (800, 1200, 2500) using a grinding and lapping machine (Buehler, Lake Bluff, IL, USA). The blocks were then polished on a Buehler wheel using 3 mm diamond paste (DP-Paste M, Struers A/S) and a satin woven acetate polishing cloth (DP-Dac, Struers A/S) for 30 minutes following another 5-minute cycle using another polishing cloth with 1 mm monocrystalline diamond suspension (MetaDi, Buehler). The mounts were cleaned in an ultra-sonic water bath after each phase, then finished with another round of ultra-sonic bath in petroleum ether (40°-60°C, analytical reagent grade, Fisher Scientific). Samples were carbon-coated using a carbon evaporation coater (HHV Auto 360), the carbon acting as a conductive layer to prevent charging.

Major and trace element compositions were determined using a wavelength-dispersive JEOL JXA-8200 electron microprobe at the Research Laboratory for Archaeology and the History of Art (RLAHA), University of Oxford, UK. An accelerating voltage of 15 kV, 10 nA beam current and 10-micron beam were used to analyse the polished samples. Peak count times were 30 s for P, Al, Na, Si, K and Ca; 40 s for Cl; and 60 s for Mg, Sr, Fe and Mn. Background counts were collected for half the peak count time either side of the peak.[120] The microprobe was calibrated using a range of mineral standards, with accuracy verified by analysing apatite secondary standards (Durango, Bamble and Wilberforce)[121] and previously analysed secondary bone standards provided by the Directorate Earth and History of Life, Royal Belgian Institute of Natural Sciences, at the start of every run. Reference materials were within ±1 standard deviation of the preferred values.[122] Analytical errors of the electron microprobe analysis (EMPA) and detection limits for the measured elements are provided in Table 1. K and Mg were in much higher concentration in the samples than in the secondary standards, meaning that their error rates presented a lower value. Thus, the standard deviation percentage (SD%) was measured for these elements which were 37.87 SD% for K and 3.83 SD% for Mg. A total of 617 measurements were taken from the outer cortical layer (OC), mid-cortical region (MC), inner cortical layer (IC), and around vascular canals (HC) on the transverse bone sections. This excludes 82 points that were removed from the dataset, because the sum of elements was less than expected in bone (total elements measured <50%) due to errors in locating and focusing the electron beam.

Element	Secondary Standards	Confidence Interval (CV)	Detection limit
P	Bamble, Durango, Bone	0.79	0.07
Na	Bamble, Durango, Bone	6.90	0.02
Cl	Bamble, Durango, Bone	3.49	0.01
K	Bone	17.22 (SD%: 37.87)	0.01
Fe	Bamble, Durango, Bone	33.99	0.01
Al	Wilberforce	1.71	0.03
Si	Bamble, Durango, Wilberforce	16.81	0.04
Sr	Bamble, Durango, Wilberforce, Bone	57.62	0.03
Mn	Bamble, Durango, Wilberforce, Bone	65.20	0.01
Mg	Bamble, Wilberforce, Bone	2.82 (SD%: 3.83%)	0.02
Ca	Bamble, Durango, Bone	0.51	0.01

Table 1 - The coefficient of variation (CV) and detection limits (D.L.) of the measured major and trace elements in the secondary standards.

2.3 Statistical Analysis

The absorption peaks, ratios from the FTIR and the elemental concentration EMPA data were analysed using Python programming language. Descriptive statistics and linear regression were used to measure the strength of the relationship between the measured changes and the PMI in both the unburnt and burnt bones, with statistical significance assessed by associated p-values ($\alpha = 0.05$). The null hypothesis was that parameter X does not increase with PMI. The coefficient of variation (CV) was used to evaluate the scattering of parameters in each group with different PMI and burning status.

Principal Component Analysis (PCA) and Linear Discriminant Analysis (LDA) were used to identify the main elements of interest and FTIR ratios were used to differentiate between PMI groups and burning states. LDA was a better statistical model for the purposes of this study. *A priori* categories in this study were state (unburnt vs burnt), PMI (0-365 days), and zone (outer-, mid-, inner-cortical, and around vascular canals). Each sample's confidence score determined the parameter based on which they

were placed into one of these categories. Multivariate analysis of variance (MANOVA) was used to examine for statistical differences on one dependent variable (PMI) by independent grouping variables (EMPA and FTIR datasets) in Statsmodels Python library. This was coupled with pairwise posthoc multivariate comparison testing (MCT) to identify which specific groups significantly differed from one another.

Datapoints below detection points (Table 4) were entered as 0.00 in the EMPA data. Both FTIR and EMPA dataframes were scaled for the analyses using Sklearn Python library. All data analyses were performed in Jupyter Notebook in Python programming language.

3. Results

3.1 FTIR Results

The spectra of unburnt and burnt bone were investigated in different regions and their associated changes were noted as a function of length of PMI and burning (Fig. 1; Table 2). A change in the intensity of peaks from 0 to 365 days PMI groups were found at several frequencies.

[insert Fig. 1 here]

Fig. 1 - The FTIR spectra of the means of each PMI group before (upper image) and after (lower image) burning. Labelled are the peak assignments of interest.

Wavenumber (cm-1)	**Functional Group**	**Mode**	**Bone Samples**	
			Unburnt	**Burnt**
3570	Apatitic hydroxyl groups ($_{vs}OH^-$)	OH stretching[79,123]	N/A	Intensity decreases with longer PMI
3600-2700	Organic fraction and water[124]	C-H and O-H stretching [125]	Convoluted bands, no peaks	N/A
2400-2300	(atmospheric) CO_2	C≡O stretching[126]	Doublet of bands (traces of CO_2 from atmosphere)	Doublet of bands (traces of CO_2 from atmosphere)
2010	Cyanamide (CH_2N_2)[8,127]	C-N stretching	Weak peak present, highest in 365-day group	Weak peak present, highest in 365-day group

1660	Amide I[79] (C=O) and water	C-O stretching and H-O-H bending	Decreases with longer PMI	Very weak bands: highest 0-day group, lowest 365-day
1550	Amide II[79] (N-H)	N-H bending	Decreases with longer PMI	Very weak bands: highest 0-day group, lowest 365-day
1250	Amide III[79] (N-H)	N-H bending	Shoulder on all groups, except a very weak peak in the 0-day group	N/A
1600-1300	Stretching modes of carbonate ions[124,128]	C-O stretching	Three broad bands with additional peaks; highest: 365-day, lowest: 0-day, mixed in between	Weak bands, highest; 0-day, lowest: 14-day
1415	B type carbonates $_{v3}(CO_3^{2-})_B$[128,129]	C-O stretching	Highest of the carbonate peaks, highest in 365-day, lowest in 0-day	Weak peaks: highest in 0-day, lowest in 365-day
1540	A type carbonates $_{v3}(CO_3^{2-})_A$[128]	C-O stretching	Overlaps with Amide II	Weak peaks: 0-day highest, 365-day lowest
1123	Extra peak, due to appearance of β-TCP [118]	P-O stretching [anti-symmetric (v3)]	No extra peak. Shoulder on the 0 and 91-day groups.	Extra peak around 1080-1090 cm-1 on all groups except 34-day group
960-1200	$_{v1,\ v3}$ (PO_4^{3-})[79]	P-O stretching [symmetric (v1) and anti-symmetrics (v3)]	No peaks, shoulders. Most intense: 365-day, least intense: 0-day	Present. Highest intensity: 0, 91, 180-day; weakest: 14-day
872-879	Carbonates (three sub-bands): type A, type B, 'labile' $_{v2}(CO_3)$ [124,130,131]	out-of-plane bending C-O	Present, but as a convolution of the three sub-bands. Highest: 365-day, weakest: 0-day. All the rest are clustered around the same absorbance value.	Present, but as a convolution of the three sub-bands. Decreases with longer PMI. Most intense: 0-day > 14-day. Other groups: clustered around the same lower value
640 - 620	Apatitic hydroxyl groups[79,132]	(OH) librational	N/A	Present. Intensity of peak: 91 > 34 > 180 > 365 >14 > 0-day
600-500	$_{v4}(PO_4^{3-})$[128,129]	P-O bending	2 peaks ($_{v3}$ splitting). Most intense: 365-day, least intense: 0-day	3 peaks ($_{v3}$ splitting and OH_{lib} band). $_{v3}$ intensity: 91 > 34 > 180 > 365 > 0 > 14-day

547	Shoulder, due to appearance of β-TCP[118]	P-O bending[128,129]	Present on all. 365-day: strong, 180-day: moderate, 91-, 34-, and 14-day: weak, 0-day: very weak	N/A

Table 2 - Identified zones of interest and their associated absorption changes on the unburnt and burnt bones.

The majority of the mean IRSF values for the unburnt bones ranged between 2.88 and 3.30, with the exception of the 365-day bone (5.04) (Suppl. 4). There was an increase in all mean IRSF values post-burning (37.77-57.27%) across all groups, except for the 365-day PMI sample, which decreased by 5.35%. In unburnt bone, the 365-day group's high IRSF value was significantly different than all other PMI group (Table 3). CV values showed very low variation across samples within the same PMI groups. IRSF gives an indication of highest reached temperature and cremation efficiency, due to increased crystallinity values. The sequence of crystallinity of the PMI groups is: 91 > 0 > 180 & 365 > 34 > 14 days. This sequence does not follow the PMI order and it is likely due to the variation in burning conditions (e.g. temperature, duration, position in the pyre), which are the dominant factors affecting crystallinity.

The results of the linear regression (Table 3) show that there was a strong positive linear correlation between IRSF and time since deposition in unburnt bone ($r=0.856$, $p<0.029$). This increase in structural ordering suggests the early post-mortem recrystallisation of bioapatite is already measurable in the first 1 year of PMI. BPI was negatively correlated with PMIs in unburnt bone ($r=-0.876$, $p<0.022$) (Table 3). Although there was no linear change in any of the proposed parameters for PMI estimation in the burnt bone, MANOVA and MCT revealed that IRSF, C/C, and CO/CO_3 ratios were significantly different in various PMI groups in burnt bone, as well as IRSF, BPI, C/C, and PHT in unburnt bone (Table 3).

FTIR Parameters	Linear Regression				Multivariate comparison of means test		
	Unburnt		**Burnt**		**PMI** (PR>F)		**State** (PR>F)
	r	**p**	**r**	**p**	**unburnt**	**burnt**	
IRSF	0.856	**0.029**	0.2	0.704	**0.000002**	**0.014**	**0.001**
C/P	-0.531	0.278	-0.557	0.251	0.505	0.561	**0.001**

BPI	-0.876	**0.022**	-0.619	0.19	**0.006**	0.638	**0.001**
API	N/A	N/A	-0.631	0.179	N/A	0.667	N/A
CO3/P	0.269	0.606	-0.049	0.926	N/A	N/A	N/A
C/C	0.08	0.879	0.096	0.855	**0.034**	**0.003**	**0.024**
CN/P	-0.701	0.12	-0.039	0.941	0.535	0.316	**0.003**
CO/CO3	-0.655	0.158	-0.519	0.29	0.16	**0.003**	**0.005**
PHT	0.679	0.138	-0.159	0.763	**0.032**	0.055	**0.001**
N/P	-0.46	0.357	-0.508	0.303	N/A	N/A	N/A
APR	-0.542	0.267	-0.492	0.321	N/A	N/A	N/A

*Table 3 – Linear regression and multivariate comparison test (MCT) on the FTIR dataset. Correlation Coefficient ('r') and p-value ('p') for each analysed FTIR parameter on the unburnt and burnt bone in the linear regression section. . H_0= X parameter does not increase with postmortem time period. ** indicates significant p-values. The MCT section shows the results of the MANOVA and multivariate comparison testing on the established FTIR ratios as a function of state (unburnt vs. burnt) and time.*

Unburnt bone at 0 and 91-day PMI displayed an extra shoulder at 1123 cm^{-1}, which is assigned for either β-TCP or Mg substitution[118]. All burnt bone had an extra peak at 1100-1080 cm^{-1}, except the 34-day post-mortem group. No burnt bone displayed a shoulder at 547 cm^{-1}, but it was a common feature in the unburnt bone, intensity ranging from strong (365-day) to very weak (0-day), which translation band also suggest Mg-OH substitutions [133]. Mg shows a non-uniform, non-linear increase in the unburnt bone through the PMI in the EMPA data.

PCA indicated that the ratios explained 81.09% of the variance in the dataset with the first (PC1) and second (PC2) principal components accounting for 66.67% and 15.00%, respectively. Loadings show that all ratios contributed to PC1, with IRSF (0.74), BPI (0.35), and CO/CO_3 (0.33) being the largest (Fig. 2), while the main contributors to discrimination by LDA was C/P for burnt bone and PHT and CN/P for unburnt bone (Suppl. 5). Both PCA and LDA differentiated between unburnt and burnt bone, but not between PMI groups.

[Insert Fig 2 here]

Fig. 2 – Loadings of the principal component analysis when using both the FTIR and EMP dataset.

3.2 WDS-EMP Results

WDS-EMP data were analysed spatially for major and trace elemental concentration (Suppl.6) of unburnt and burnt bone at different PMIs. Variations in elemental concentrations as a function of time in the experimental bone are visualised in Fig. 3. The most highly variable zones in unburnt bone across all elements were the OC (0.60) and HC (0.50), while IC (0.49) and MC (0.46) were the lowest. The mid-cortical and the inner cortical zones showed the lowest variability across all samples.

In the archaeological cremated bone (KILT) P and Ca remained relatively stable in all zones, while K, Fe, Al, Si, Sr, Mn, and Mg display very high values in the outer cortical layers, suggesting diffusion of elements from the soil (Fig. 4). The highest CV scores were recorded for Sr, especially in the outer cortical layers.

[Insert Fig 3 here]

Fig. 3 – Average elemental concentration (wt %) of the experimental bones using the EMPA data. Mean ± 2 standard errors for each measured element as a function of time in unburnt and burnt bone.

[Insert Fig 4 here]

Fig. 4 – Average elemental concentration (wt %) of the Neolithic cremated human remains for each zone. Mean ± 2 standard errors for each measured major and trace element in archaeological cremated bone. The backscattered electron microscopy (BSEM) image represents an example of a bone cross section.

Linear regression analysis (Table 4) shows that in unburnt bone only K, Mn, and Mg in unburnt bone and Na, Cl, and K changed in a linear fashion with time. K was the only element that decreased both in the unburnt and burnt bone sections overall, and separately in the IC and HC zones. There were no significant trends in the Ca/P ratios and all zones presented similar values (between 1.23 and 1.29) while the archaeological samples were insignificantly higher (1.35).

Element	Location	Linear Regression				Multivariate Comparison Test (MCT)		
		Unburnt		Burnt		PMI		
		r	p	r	p	Unburnt	Burnt	State
P2O5	OC	0.602	0.206	0.204	0.699			
	MC	0.246	0.638	-0.276	0.597			
	IC	0.217	0.68	-0.572	0.236			
	HC	0.063	0.905	-0.428	0.397			
	All	**0.277**	**0.19**	**-0.284**	**0.179**	0.419	**0.000	**0.001
Na2O	OC	-0.172	0.745	-0.676	0.141			
	MC	-0.436	0.388	-0.873	**0.023			
	IC	0.561	0.247	-0.889	**0.018			
	HC	0.236	0.652	-0.872	**0.023			
	All	**-0.051**	**0.813**	**-0.744**	****0.000**	0.061	**0.000	**0.001
Cl	OC	-0.397	0.436	0.830	**0.041			
	MC	-0.099	0.852	0.702	0.120			
	IC	-0.142	0.789	0.843	**0.035			
	HC	-0.009	0.986	0.801	0.055			
	All	**-0.162**	**0.449**	**0.690**	****0.000**	**0.000	**0.000	**0.001
K2O	OC	-0.655	0.158	-0.54	0.269			
	MC	-0.603	0.205	-0.666	0.149			
	IC	-0.834	**0.039	-0.810	**0.050	**6.05E-26	**9.15E-23	**0.001
	HC	-0.551	0.257	-0.804	0.054			
	All	**-0.552**	****0.005**	**-0.578**	****0.003**			
FeO	OC	-0.413	0.416	-0.397	0.436			
	MC	0.614	0.195	-0.097	0.855			
	IC	-0.153	0.773	0.011	0.983	0.767	0.302	0.839
	HC	-0.493	0.321	-0.395	0.438			
	All	**-0.160**	**0.454**	**-0.251**	**0.238**			
Al2O3	OC	-0.304	0.558	-0.027	0.96			
	MC	-0.497	0.316	0.502	0.311			
	IC	-0.441	0.382	0.690	0.129	0.633	0.209	0.900
	HC	0.715	0.111	-0.423	0.403			
	All	**-0.127**	**0.555**	**-0.171**	**0.424**			
SiO2	OC	-0.498	0.315	-0.780	0.067			
	MC	-0.584	0.223	-0.519	0.291			
	IC	-0.391	0.443	-0.507	0.304	0.283	0.493	0.497
	HC	-0.045	0.932	-0.370	0.470			
	All	**-0.242**	**0.255**	**-0.206**	**0.335**			
SrO	OC	0.178	0.736	0.025	0.963			
	MC	-0.255	0.625	0.215	0.682	**0.000	**3.03E-32	0.470
	IC	0.086	0.872	-0.052	0.922			
	HC	0.128	0.809	0.023	0.966			

	All	**0.027**	**0.899**	**0.054**	**0.804**			
MnO	OC	0.637	0.173	-0.473	0.344	0.952	0.692	**0.031
	MC	-0.873	**0.023	0.123	0.817			
	IC	-0.567	0.241	0.137	0.795			
	HC	0.523	0.287	-0.085	0.872			
	All	**0.127**	**0.553**	**-0.062**	**0.772**			
MgO	OC	0.709	0.115	0.182	0.731	**0.048	**0.000	**0.003
	MC	0.402	0.429	0.621	0.189			
	IC	0.780	0.068	-0.418	0.409			
	HC	0.480	0.335	0.379	0.458			
	All	**0.456**	****0.025**	**0.138**	**0.52**			
CaO	OC	0.753	0.084	0.642	0.169	0.089	**0.001	**0.001
	MC	0.137	0.795	-0.555	0.253			
	IC	0.078	0.884	-0.668	0.147			
	HC	0.071	0.894	-0.637	0.174			
	All	**0.286**	**0.176**	**-0.354**	**0.090**			

*Table 4 – Linear regression and multivariate comparison test on the EMPA data. Correlation Coefficient ('r') and p-value ('p') are given for each analysed element in unburnt and burnt bone for the linear regression. H_0= X parameter does not increase with postmortem time period. ** indicates significant p-values. HC = around vascular canals; OC = outer cortical; MC = mid-cortical; IC = inner cortical zones. In the multivariate comparison test, p values are derived from both MANOVA and multivariate comparison testing.*

[Insert Fig 5 here]

Fig. 5 – Potassium wt% content in experimental unburnt (upper) and burnt (lower) bone by zone.

PCA showed that the first principal component (PC1) explained 93.49% of the variance and the second principal component (PC2) explained 4.19%, with the key discriminators being Ca and P (Fig. 2). LDA was used to reduce the features (elements), classify samples, and subsequently visualising the classification according to the defined categories (state, PMI, zone). When the data were transformed into a two-feature (unburnt vs burnt) linear discriminant dataset, the two states were clearly differentiated (Fig. 6A). LDA did not clearly differentiate between the PMI groups, with slightly more separation of PMIs in unburnt bone (Fig. 6B). MANOVA and MCT showed that P, Na, Cl, K, Mn, Mg,

and Ca were significantly associated with burning, while Fe, Si, Sr, and Al were not (Table 4). An overall significant difference was observed between PMI groups in Cl, K, Sr, and Mg levels in unburnt bone, and in P, Na, Cl, K, Sr, Mg, and Ca values in burnt bone (Table 4). The fresh group differed significantly in K values from all other PMI groups in both unburnt and burnt bone by MANOVA and MCT.

[Insert Fig 6 here]

Fig. 6 – Linear discriminant analysis (LDA) on the EMPA dataset. ***A****: Separation of unburnt and burnt bone by LDA. Contributions: 'Al2O3': 0.244, 'CaO': -6.882,'Cl': 3.216,'FeO': 0.07,'K2O': 0.607,'MgO':-1.036,'MnO': -0.056, 'Na2O': -0.545,'P2O5': -3.97,'SiO2': -0.902,'SrO': 0.199, 'Total': 13.08.* ***B:*** *Clusters created by LDA of the unburnt (left) and burnt (right) PMI groups.*

Discussion

This study on the early diagenesis and burning of bioapatite has shown that both structural and chemical changes are observable after only 1 year PMI. Potassium elemental concentration decreased with PMI and survived burning, making it the best discriminator between bone burnt fresh and partially decomposed. This decrease compared to experimental bone suggests that endogenous K had decayed prior to cremation in the Neolithic bone, thus the bodies might have been left to decompose prior to further funerary treatment. While decrease in carbonates and increase in crystallinity were documented in only 1 year of surface exposure, these were masked by burning. Ca, P, Fe, Al, Si, and Sr did not significantly change with heat-treatment and Fe, Al, Si, and Sr were not associated with time since deposition either.

Crystallinity increases in a linear fashion with PMI in unburnt bone and burnt bone shows higher crystallinity compared to unburnt bone. This is in agreement with the literature (e.g., [8,95]), except the 365-day burnt group where results show a slight decrease, which may be the result of the bone's already higher crystallinity or small-scale temperature variation across individual bones. The lack of linear increase in burnt bone crystallinity with time suggests that burning overrides the increase in IRSF

due to early diagenesis in the first 6 months of the PMI. As crystallinity increased, carbonate content decreased in a linear fashion in the unburnt bone, in line with other studies.[134,135] Keenan and Engel[135] documented significant carbonate loss at 3 years PMI, with insignificant decrease after 1 year but increase compared to that value in 2 years, while here A and B carbonates to phosphate ratios showed a significant linear decrease throughout only a year PMI. However, B type carbonates only significantly changed prior to 3 months PMI compared to the 365-day group. Burning, again, obscured the effects of early diagenesis of carbonate loss.

β-TCP signals the thermal decomposition of the apatite phase and should be detectable in bones burnt at >700°C,[97,98,136] which was reached in this study for a short duration. There is an extra peak at ~1100-1080 cm^{-1} on all burnt bone spectra, which might be due to a shift in the spectra and might still represent β-TCP. However, the lack of a shoulder at 547 cm^{-1} suggests otherwise. Surprisingly, all unburnt bone displayed a shoulder at 547 cm^{-1}. These shoulders cannot be due to β-TCP in unburnt bone, but are probably due Mg substitutions for Ca.[118] However, there were no outstanding elevated levels of Mg in the unburnt bone (unburnt mean Mg levels ranged between 0.01 and 0.82 wt%). Mg values in all zones are slightly higher in the 180- and 365-day groups than those with shorter PMIs, suggesting a non-uniform, non-linear increase. However, Mg-values were highly variable in burnt bone. With a melting point of 650°C, this might be due to the burning efficiency of the different fire events. Therefore, β-TCP as a thermal decomposition product might not have occurred, but Mg ions might have increased despite its reduced competitiveness in substituting due to the crystal lattices' more accommodating nature for sodium and potassium.[137] Another possibility is that β-TCP did appear as a thermal decomposition product, but post-cooling it was not possible to detect, as it is not thermally stable.[138]

As the bones were burnt in an outdoor fire, burning efficiency was variable. Burning efficiency could be estimated for the different PMI groups from the N/P ratios and IRSF. The sequence from highly efficient to less efficient from N/P was 91- and 180-day > 365-day > 34-day > 0-day > 14-day, while from IRSF data it was 91-day > 0-day > 180- and 365-day > 34-day > 14-day. The differing placement of the 0-day group in the two sequences might be due to the placement of the different fat-

content of the individual fresh legs, since fat acts as a fuel during burning, increasing temperature when more fat is present and resulting in higher crystallinity. MANOVA results confirmed that all FTIR ratios designed to assess cremation efficiency[37,95,112] differ significantly in unburnt and burnt bone. In both cases, the 91-day group was the most efficiently cremated and the 14-day group the least. This might explain why only the 14-day and the 0-day groups showed significantly different values in P in burnt bone. Ca and P, the two major elements in bone, were otherwise insignificant in both the unburnt and burnt groups. Sr was significantly different in the most efficiently burnt group (91-day) than in all others, but this difference was present in its unburnt state as well; thus it was not due to burning.

Other than Mn, the increase in all other element's atomic percentage is higher in burnt 0-day (fresh) bone than in unburnt fresh bone. However, it appears this is due to the decrease in organic content and thus does not essentially indicate a real increase in the mineral phase. Ca, P, Fe, Al, Si, and Sr changes through the PMI stages in the same fashion in unburnt and burnt bone, meaning they are not highly affected by burning at ≤750°C and their amount in burnt bone is representative of their pre-burnt levels. The results for Sr are in agreement with those of Snoeck *et al.*,[8] who did not find changes in Sr isotopic signals following experimental cremation. Fe showed an initial increase at 14-day PMI and a sharp decrease thereafter, which is due to soft tissue putrefaction and aligns with the literature.[42]

Only three elements (K, Na, Cl) were found to be affected by time since deposition in the first year PMI. Potassium and sodium are associated with moisture in bone and their decrease signifies dehydration.[42] Here, potassium was the most useful element in differentiating between fresh (0-day) and all other PMI groups in unburnt bone. In addition, K showed an overall linear decrease in both unburnt and burnt bone area for all zones combined. The unburnt group's potassium values suggest rapid depletion of K in 2 weeks (from mean 0.16 wt% to mean 0.06 wt%), after which depletion slowed down. Environmental factors might have altered the rate of depletion in the OC and IC zones. After 34 days, bone had a higher K-value in the OC zones, which coincides with the time at which the specimens started to be noticeably partially submerged into the soil. The burnt experimental bone always had higher K-levels than unburnt, but followed the same pattern of depletion. Although KOH has a relatively low melting point (360 °C), it was found in apatitic aorta deposits burnt at 720 °C,[139] suggesting that it

is bound to the crystal. K was previously found to be localised in the removed organic bone material[140] and was suggested to be present mainly in a labile state, meaning it is localised on the mineral crystal surface with low migration activity.[139] However, the latter study's limitations included a more limited detection limit of EDS and the inability to evaluate the contributions to the labile fraction corresponding to surface-localised water-soluble compounds related to the organic matrix. Since organic material was removed by burning in the present study's bones, meaning that the oxidation of carbon was complete (assessed by the white colour of calcined bones without black ash/carbon left behind), but K was still detectable by EMPA, it is possible that K integrates into the crystal lattice. The 0-day burnt bioapatite samples always had K-values ≥0.20 wt%, while after 14 days this decreased to <0.14 wt% in all areas. The OC zones also showed depletion but at a slower rate than other areas. After 3 months, all K concentrations at IC, MC, and HC zones were ≤0.06 wt% and <12 wt% at OC areas. Thus, K-levels of $<0.07 \pm 0.001$ wt% in the inner and mid-cortical zones, and around vascular canals of burnt bone suggest that the corpse was not burnt immediately after death, but after around 3 months. The outer cortical zones might show higher K concentrations due to uptake of potassium from the soil. It has to be noted that these bones were surface exposed and that dehydration would be expected to be slower had they been buried. In the Neolithic human bone fragments, endogenous K was below detection limit in the mid-cortical bone sections. Exogenous K (mean 0.08 wt%) from the soil might have diffused into the outer cortical layers and to a lesser degree from the IC end and through the HC zones. Since bioapatite is less susceptible to changes post-burning, due to increased crystallinity,[8,61,101,141] this might mean that potassium essentially depleted in the Neolithic samples prior to cremation. Therefore, these bodies might have been left to decompose prior to cremation, to a degree that endogenous potassium was no longer present. Based on the experimental results of this study, in which K-values were never below the detection point at any zone, the postmortem interval prior to cremation in the archaeological bone can be suggested to have been >1 year.

Sodium is also associated with extracellular fluid in the body.[42] The 0-day burnt group showed higher values than the unburnt group, which is in agreement with Ellingham et al.[70] In the experimental burnt samples there was a slight decrease between the 0-day (0.54 wt%) and 14-day (0.46 wt%) groups,

after which it remained stable (0.45 – 0.48 wt%). Previously, Na was shown to have a tendency of mass transfer, leaving the crystals at 720 °C and increasing at 760 °C, which was suggested to be due to the reversible exchange of CO_3^{2-}.[139] Here, Na showed a linear decrease with time in heated bones. The decrease of Na in the EMPA data is confirmed and supported by the decrease of CO_3 ions in the FTIR data.[142] The initial value was 54% lower than in modern human bone reported by Elliott [45]. This discrepancy might be due to inter-species differences in calcium-substituting ions, such as Na, but studies on them are sparse.[143] The Na value of 0.47 wt% for the Neolithic bone is consistent with that of unburnt archaeological bone reported in the literature.[144] The burnt bone demonstrated that MC, IC, and HC zones had similar Na-values, while OC zone was depleted. Normally, Na leaches out of the layers of bone closest to the environment over time,[144,145] but these bones were broken. Nevertheless, it seems to explain why the experimental burnt bone had higher Na values in the OC zones 1 year post-mortem than the archaeological samples.

Cl values in burnt bone behaved almost inversely proportional to unburnt bone over time. Cl-enriched phases might appear in early diagenetic bone through the incorporation of Cl^- facilitated by the protonation of hydroxyl ions,[54] and/or by burning above 600°C,[146] up to <800 °C in defleshed bone and <900°C in fleshed bone.[70] OH sites in bone can be substituted with Cl.[142] An OH-Cl peak was observed in the FTIR spectra of the burnt bones in all PMI groups, suggesting that Cl substitution for OH started in these bones. Our results are supported by the agreement between the EMPA and the FTIR results and previous studies' results showing Cl incorporation when HAP is heated above 600°C.[146]

PCA and LDA formed clearly separate clusters of unburnt and burnt groups, but were unable to distinguish between PMI groups. C/P, PHT and CN/P were the main discriminating ratios between the state of bone. Thus, FTIR is a useful technique in differentiating between unburnt and burnt bone, but it cannot detect early diagenesis up to 1 year postmortem in burnt bone. The main discriminating chemical elements between unburnt and burnt bone were Ca and Cl by LDA, and Ca and P by PCA.

Ca/P molar ratios remained fundamentally constant not only during soft tissue putrefaction,[69] but also at 1 year PMI. The fact that this ratio did not present significant alterations with burning makes

it a characteristic signature of bone, further supported by the similar Ca/P ratios of the archaeological and experimental burnt bone. Ratios were much lower than for stoichiometric HAp, due to the lattice housing carbonates and other elements.[45] Both Ca and P remained stable during the entire PMI. For Ca, this is in agreement with Reidsma et al.,[43] but in contrast to findings by Subirà and Malgosa[81] and McKinnon et al.[99]. Although a decrease in C/P ratio had been documented after 1 year of burial,[135] here C/P ratios (from the FTIR dataset) did not change significantly with PMI, suggesting a stable ratio of carbonate to phosphate during the studied PMI in the same unburnt or burnt groups. The discrepancy with Keenan and Engel's[135] results might be due to the fact that their experimental alligator bones had evidence of microbial bioerosion, while this was not present in this study's bones.[39] Nevertheless, time since deposition does not seem to be the driving cause of C/P variation.

The outer cortical layer's highest variation in elements in unburnt bone demonstrates that exogenous elements diffuse into the bone in less than 1 year and endogenous elements are lost. However, zones around the vascular canals show the most varied elemental chemistry once bone is burnt. The high variability in concentration around osteons aligns with a microsampling study of unburnt bone by Scharlotta et al.[147] which found the presence of diagenetically unaltered zones further from the osteons. K, Si, Al, and Fe were barely detectable in the mid-cortical section in the archaeological bone; while the levels of these elements were high in the OC layers. However, in the experimental bone, the MC section did exhibit changes in elemental concentration with time. In other words, the mid-cortical section is more resistant than other areas of the bone, but it is also taphonomically altered, evidenced in <1 year postmortem.

Conclusion

Fire drastically changes the morphological and chemical profile of bone making it notoriously difficult to derive information about circumstances surrounding death and deposition or burial of an individual. This includes how cultures treated their dead prior to and during cremation, and how cause and manner of death are identified after burning in forensic cases. Our investigation indicates that crystallinity increases in unburnt bone are detectable during the first year postmortem. B-type carbonate

content decreased rapidly in the first 3 months PMI in unburnt bone, after which it slowed down. Both changes are masked by burning. The thermal decomposition of the apatite phase did not occur post-burning from the lack of β-TCP signals in the IR spectra. The presence of these signals in unburnt bone suggests Mg substitutions, supported by the non-uniform, non-linear increase of Mg values with time from the EMPA data.

Major (Ca, P) and some trace elements (Fe, Al, Si, Sr) were not significantly associated with thermal treatment, while Fe, Al, Si, and Sr were not associated with the PMI. K, Na, Mg, and Cl were the only elements associated with time since deposition in the experimental bone. Potassium showed a potential to estimate the late postmortem interval/early diagenesis in both unburnt and burnt bone in the first year postmortem. Potassium rapidly depleted in bone after 2 weeks and continued to decrease over 1 year PMI. It is proposed here that if the K-values are under 0.07 ±0.01 wt% in the inner and mid-cortical zones of burnt bone then they were not burnt subsequently after death, but after at least 3 months decomposition in a surface exposed environment, or after a few months/years if buried, since burial slows down dehydration. Since K was present in calcined bones, it is proposed here that it might not exclusively be present in the organic phase of bones. In the Neolithic human cremated bones endogenous potassium is below detection limits. Therefore, if the bioapatite crystal structure truly become thermodynamically stable after burning at high temperatures as previous studies indicate [8,61,101], then it suggests that cremation of these corpses were delayed by at least some weeks following death.

Sodium, which is also associated with the extracellular fluid, rapidly decreased by 2 weeks in both unburnt and burnt bone, after which it remained stable in the former, but continued to decrease at a higher rate in the latter. The decrease of Na in the burnt bones was also confirmed by the decrease of CO_3 ions. The increase of Cl in the burnt bones with time was confirmed by the EMPA data and the start of the Cl substitutions for OH by the OH-Cl peaks in the FTIR data.

PCA and LDA were moderately successful at differentiating between unburnt and burnt bone, but not between PMIs of up to 1 year. C/P, PHT, and CN/P from the FTIR and Ca, Cl, and P from the EMPA were the best discriminators for unburnt vs burnt state of bone. This study demonstrates that

Ca/P molar ratios do not change significantly due to PMI or burning in the experimental and only insignificantly change in the archaeological bone. However, C/P ratios might be dependent on the presence of microbial bioerosion rather than the time since deposition. Elemental chemistry analysis demonstrated that the mid-cortical zone is the least affected by contamination in both a modern and archaeological timescale.

This study has relevance for the assessment of postmortem interval, deposition environment, and time of burning in analysis of archaeological cremated bones and of burnt human remains in forensic cases.

Supporting Information

Please find supplementary material provided with this file.

Acknowledgments

We would like to thank Dr Victoria Smith for her help and assistance on the electron microprobe and Sophie Decree from the Directorate Earth and History of Life, Royal Belgian Institute of Natural Sciences for providing the secondary bone standards for the EMPA analysis of this study. We would also like to thank the team at Wytham Woods, Oxfordshire, UK for allowing us to conduct the taphonomy experiment and outdoor burning at their site. The Kiltierney samples were provided by the Environment and Heritage Service, Northern Ireland. We would also like to thank the anonymous reviewers for the valuable comments and improvements made to the paper.

Notes

The authors declare no conflict of interest.

Funding

The authors disclosed receipt of the following financial support for the research of this article: This work was supported by the Meyerstein Foundation, School of Archaeology, University of Oxford.

Conflict of Interest Declaration

The authors declare that there is no conflict of interest.

References

1. Symes SA, Rainwater CW, Chapman EN, et al. Patterned thermal destruction of human

remains in a forensic setting. In: Schmidt CW, Symes SA (eds) *The Analysis of Burned Human Remains*. Boca Raton, 2008, pp. 15–55.

2. Bontrager AB, Nawrocki SP. *Cremains from the Fox Hollow Farm Serial Homicide Site*. Elsevier Ltd. Epub ahead of print 2012. DOI: 10.1016/B978-0-12-800451-7.00013-9.

3. Garrido-Varas C, Intriago-Leiva M. The interpretation and reconstruction of the post-mortem events in a case of scattered burned remains in Chile. In: Thompson T (ed) *The Archaeology of Cremation: burned human remains in funerary studies*. Havertown: Oxbow Books, 2015, pp. 227–242.

4. Stiner MC, Kuhn SL, Weiner S, et al. Differential Burning, Recrystallization, and Fragmentation of Archaeological Bone. *J Archaeol Sci* 1995; 22: 223–237.

5. Bennett JL. Thermal alteration of buried bone. *J Archaeol Sci* 1999; 26: 1–8.

6. Dibble H, Berna F, Goldberg P, et al. A Preliminary Report on Pech de l'Azé IV, Layer 8 (Middle Paleolithic, France). *Paleoanthropology* 2009; 2009: 182–219.

7. Gonçalves D, Thompson TJU, Cunha E. Implications of heat-induced changes in bone on the interpretation of funerary behaviour and practice. *J Archaeol Sci* 2011; 38: 1308–1313.

8. Snoeck C, Lee-Thorp JA, Schulting RJ. From bone to ash: Compositional and structural changes in burned modern and archaeological bone. *Palaeogeogr Palaeoclimatol Palaeoecol* 2014; 416: 55–68.

9. Théry-Parisot I. Fuel Management (Bone and Wood) During the Lower Aurignacian in the Pataud Rock Shelter (Lower Palaeolithic, Les Eyzies de Tayac, Dordogne, France). Contribution of Experimentation. *J Archaeol Sci* 2002; 29: 1415–1421.

10. Schiegl S, Goldberg P, Pfretzschner H-U, et al. Paleolithic burnt bone horizons from the Swabian Jura: Distinguishing betweenin situ fireplaces and dumping areas. *Geoarchaeology* 2003; 18: 541–565.

11. Clark JL, Ligouis B. Burned bone in the Howieson's Poort and post-Howieson's Poort Middle Stone Age deposits at Sibudu (South Africa): behavioral and taphonomic implications. *J Archaeol Sci* 2010; 37: 2650–2661.

12. Yravedra J, García-Vargas E, Maté-González MÁ, et al. The use of Micro-Photogrammetry and Geometric Morphometrics for identifying carnivore agency in bone assemblages. *J Archaeol Sci reports* 2017; 14: 106–115.

13. Waterman DM, Wells C, Northover JP. The Excavation of a Court Cairn at Tully . County Fermanagh. *Ulster J Archaeol* 2017; 41: 3–14.

14. Dowd MA. The use of caves for funerary and ritual practices in Neolithic Ireland. *Antiquity* 2008; 82: 305–317.

15. Cooney G. The Role of Cremation in Mortuary Practice in the Irish Neolithic. In: Kuijit I (ed) *Transformation by Fire: The Archaeology of Cremation in Cultural Context. Amerind Studies in Archaeology*. University of Arizona Press, 2014, pp. 189–206.

16. Wells C. Notes on Cremated Bones from Tully Court Cairn. *Ulster J Archaeol* 1978; 41: 13–14.

17. Chesterman JT. Investigation of the human bones from Quanterness. In: Renfrew C (ed) *Investigations in Orkney*. London: The Society of Antiquaries of London, 1979, pp. 97–111.

18. Renfrew C. *Investigations in Orkney*. London: The Society of Antiquaries of London, 1979.

19. Carr G, Knüsel C. The ritual framework of excarnation by exposure as the mortuary practice

of the early and middle Iron Ages of central southern Britain. In: Gwilt A, Haselgrove C (eds) *Reconstructing Iron Age societies: new approaches to the British Iron Age*. Oxford: Oxbow Books, 1997, pp. 167–173.

20. Mckinley J. *The Anglo-Saxon cemetery at Spong Hill, North Elmham. Part VIII: the cremations*. Norfolk, Museums Service, 1994.

21. Mckinley J. Human remains and diet. In: Mercer R, Healy F (eds) *Hambledon Hill, Dorset, England, Volumes 1 and 2 -- Excavation and survey of a Neolithic Monument Complex and its Surrounding Landscape*. Swindon: JSTOR, 2008, pp. 477–535.

22. McKinley JI. Cremation burials. In: Barber B, Bowsher D (eds) *The eastern cemetery of Roman London: Excavations 1983-90 MoLAS Mon. 4*. London: Museum of London Archaeology Service, 2000, pp. 254–277.

23. Mckinley J. Excavations at Ham Hill, Montacute, Somerset 1994 and 1998. *Somerset Archaeol Natur Hist*; 142.

24. Wells LH. Report on the inhumation burials from the West Kennet barrow. *Piggott* 1962; 79–89.

25. Piggott S. *The West Kennet Long Barrow excavations 1955-56*. 1962.

26. Booth TJ, Brück J. Death is not the end: radiocarbon and histo-taphonomic evidence for the curation and excarnation of human remains in Bronze Age Britain. *Antiquity* 2020; 94: 1186–1203.

27. Carr G. Excarnation to cremation: continuity or change? In: Haselgrove C, Moore T (eds) *The Later Iron Age in Britain and Beyond*. Oxford: Oxbow, 2007, pp. 446–455.

28. Niblett R. *The excavation of a ceremonial site at Folly Lane, Verulamium*. London: Society for the Promotion of Roman Studies, 1999.

29. Grévin G, Baud C, Susini A. Etude anthropologique et paléopathologique d ' un adulte inhumé puis incinéré provenant du site de Pincevent (Seine-et-Marne). 1991; 77–87.

30. Lambot B, Friboulet M, Méniel P. Le site protohistorique d'Acy Romance (Ardennes) II. Les nécropoles dans leur contexte régional 1986-1988-1989. *Reims Mémoire la Société Archéologique Champenoise*; 8.

31. Baby RS. Hopewell Cremation Practices. *Pap Archaeol Ohio Hist Soc* 1954; 1–7.

32. Binford LR. An analysis of cremations from three Michigan sites. *Wisconsin Archaeol* 1963; 44: 98–110.

33. Buikstra JE, Swegle M. Bone modification due to burning: experimental evidence. In: Bonnichsen R, Sorg M (eds) *Bone modification*. College Station, TX: The Centre for the Study of the First Americans, 1989, pp. 247–58.

34. Spennemann DHR, Colley SM. Fire in a Pit: the effects of burning on faunal remains. *Archaeozoologia* 1989; 3: 51–64.

35. Etxeberria F. Aspectos macroscópicos del hueso sometido al fuego: revisión de las cremaciones descritas en el País Vasco desde la arqueologia. *Munibe* 1994; 46: 111–116.

36. Whyte T. Distinguishing remains of human cremations from burned animal bones. *J F Archaeol* 2001; 28: 437–448.

37. Thompson TJU. Heat-induced dimensional changes in bone and their consequences for forensic anthropology. *J Forensic Sci* 2005; 50: 185–193.

38. Lemmers SAM, Gonçalves D, Cunha E, et al. Burned Fleshed or Dry ? The Potential of Bioerosion to Determine the Pre-Burning Condition of Human Remains. *J Archaeol Method Theory* 2020; 27: 972–991.

39. Végh EI, Czermak A, Márquez-Grant N, et al. Assessing the reliability of microbial bioerosion features in burnt bones: A novel approach using feature-labelling in histotaphonomical analysis. *J Archaeol Sci Reports* 2021; 37: 102906.

40. Kohn MJ, Moses RJ. Trace element diffusivities in bone rule out simple diffusive uptake during fossilization but explain in vivo uptake and release. *Proc Natl Acad Sci* 2013; 110: 419.

41. Keenan SW, Engel AS. Early diagenesis and recrystallization of bone. *Geochim Cosmochim Acta* 2017; 196: 209–223.

42. Walden SJ, Mulville J, Rowlands JP, et al. An Analysis of Systematic Elemental Changes in Decomposing Bone. *J Forensic Sci* 2018; 63: 207–213.

43. Reidsma F., van Hoesel A, van Os BJ., et al. Charred bone : Physical and chemical changes during laboratory simulated heating under reducing conditions and its relevance for the study of fire use in archaeology. *J Archaeol Sci reports* 2016; 10: 282–292.

44. Rogers K, Zioupos P. The Bone Tissue of the Rostrum of a Mesoplodon Densirostris Whale: a Mammalian Biomineral Demonstrating Extreme Texture. *J Mater Sci Lett* 1999; 18: 651–654.

45. Elliott JC. Calcium phosphate biominerals. In: Kohn MJ, Rakovan J, Hughes JM (eds) *Phosphates: Geochemical, Geobiological and Material Importance, Reviews in Mineralogy and Geochemistry, vol. 48, Mineralogical Society of America*. Washington, DC, 2002, pp. 427–454.

46. Caruso V, Marinoni N, Diella V, et al. Bone diagenesis in archaeological and contemporary human remains: an investigation of bone 3D microstructure and minero-chemical assessment. *Archaeol Anthropol Sci* 2020; 12: 162.

47. Rey C, Combes C, Drouet C, et al. Nanocrystalline apatites in biological systems: characterisation, structure and properties. *Materwiss Werksttech* 2007; 38: 996–1002.

48. Li Z, Pasteris JD. Chemistry of bone mineral, based on the hypermineralized rostrum of the beaked whale Mesoplodon densirostris. *Am Mineral* 2014; 99: 645.

49. Bergslien ET, Bush M, Bush PJ. Identification of cremains using X-ray diffraction spectroscopy and a comparison to trace element analysis. *Forensic Science International* 2008; 175: 218–226.

50. Zapanta Legeros R. Apatites in biological systems. *Prog Cryst growth Charact* 1981; 4: 1–45.

51. Fernández-Jalvo Y, Andrews P. *Atlas of taphonomic identifications : 1001+ images of fossil and recent mammal bone modification*. Dordrecht, 2016.

52. Márquez-Grant N, Schotsmans EM, Forbes S. *Taphonomy of human remains : forensic analysis of the dead and the depositional environment*. Chichester, England, 2017.

53. Sponheimer M, Lee-Thorp JA. Isotopic evidence for the diet of an early hominid, Australopithecus africanus. *Science* 1999; 283: 368.

54. Keenan SW. From bone to fossil: A review of the diagenesis of bioapatite. *Am Mineral* 2016; 101: 1943–1951.

55. Child A. Towards and Understanding of the Microbial Decomposition of Archaeological Bone in the Burial Environment. *Journal of Archaeological Science* 1995; 22: 165–174.

56. Harbeck M, Grupe G. Experimental chemical degradation compared to natural diagenetic

alteration of collagen: Implications for collagen quality indicators for stable isotope analysis. *Archaeol Anthropol Sci* 2009; 1: 43–57.

57. Keenan SW, Engel AS, Roy A, et al. Evaluating the consequences of diagenesis and fossilization on bioapatite lattice structure and composition. *Chem Geol* 2015; 413: 18–27.

58. Kohn MJ. Models of diffusion-limited uptake of trace elements in fossils and rates of fossilization. *Geochim Cosmochim Acta* 2008; 72: 3758–3770.

59. Berna F, Matthews A, Weiner S. Solubilities of bone mineral from archaeological sites: the recrystallization window. *J Archaeol Sci* 2004; 31: 867–882.

60. Wright LE, Schwarcz HP. Infrared and Isotopic Evidence for Diagenesis of Bone Apatite at Dos Pilas, Guatemala: Palaeodietary Implications. *J Archaeol Sci* 1996; 23: 933–944.

61. Trueman CN., Behrensmeyer AK, Tuross N, et al. Mineralogical and compositional changes in bones exposed on soil surfaces in Amboseli National Park, Kenya: diagenetic mechanisms and the role of sediment pore fluids. *J Archaeol Sci* 2004; 31: 721–739.

62. Benmansour NZRZM. Determination of 210 Pb in human skeletal remains from Morocco : implications for time since death assessment. 2012; 315–319.

63. Gallello G, Kuligowski J, Pastor A, et al. Biological mineral content in Iberian skeletal cremains for control of diagenetic factors employing multivariate statistics. *J Archaeol Sci* 2013; 40: 2477–2484.

64. Marín Arroyo A., Landete Ruiz M., Vidal Bernabeu G, et al. Archaeological implications of human-derived manganese coatings: a study of blackened bones in El Mirón Cave, Cantabrian Spain. *J Archaeol Sci* 2008; 35: 801–813.

65. López-Costas O, Lantes-Suárez Ó, Martínez Cortizas A. Chemical compositional changes in archaeological human bones due to diagenesis: Type of bone vs soil environment. *J Archaeol Sci* 2016; 67: pp43-51.

66. Schutkowski H, Herrmann B, Grupe G. Diet , Status and Decomposition at Weingarten : Trace Element and Isotope Analyses on Early Mediaeval Skeletal Material. 1999; 675–685.

67. Keenan SW, Engel AS. Reconstructing diagenetic conditions of bone at the Gray Fossil Site, Tennessee, USA. *Palaeogeography, Palaeoclimatology, Palaeoecology* 2017; 471: 48–57.

68. Zazzo A, Lécuyer C, Mariotti A, et al. (formula presented) substitution in hydroxyapatite: Theory and experiment. *Phys Rev B - Condens Matter Mater Phys* 2020; 2148: 87–100.

69. Ezzo JA. Putting the chemistry back into archaeological bone chemistry analysis -- modeling potential palaeodietary indicators. *J Anth Arch* 1994; 13: 1–34.

70. Ellingham STD, Thompson TJU, Islam M. Scanning Electron Microscopy–Energy-Dispersive X-Ray (SEM/EDX): A Rapid Diagnostic Tool to Aid the Identification of Burnt Bone and Contested Cremains. *J Forensic Sci* 2018; 63: 504–510.

71. Williams CT. Alteration of Chemical Composition of Fossil Bones by Soil Processes and Groundwater. In: G. G, B. H (eds) *Trace Elements in Environmental History. Proceedings in Life Sciences*. Springer, Berlin, 1988, pp. 27–40.

72. Trueman CN, Tuross N. Trace Elements in Recent and Fossil Bone Apatite. *Rev Mineral Geochemistry* 2002; 48: 489–521.

73. Trueman CN. Chemical taphonomy of biomineralized tissues. *Palaeontology* 2013; 56: 475–486.

74. Pate FD, Hutton JT. The use of soil chemistry data to address post-mortem diagenesis in bone

mineral. *Journal of Archaeological Science* 1988; 15: 729–739.

75. Lambert JB, Xue L, Buikstra JE. Inorganic analysis of excavated human bone after surface removal. *J Archaeol Sci* 1991; 18: 363–383.

76. Muñoz M, Villar I, García-erce JA. An update on iron physiology. 15. Epub ahead of print 2009. DOI: 10.3748/wjg.15.4617.

77. Millard AR, Hedges RE. A diffusion-adsorption model of uranium uptake by archaeological bone. *Geochim Cosmochim Acta* 1996; 60: 2139–2152.

78. de Winter NJ, Snoeck C, Schulting R, et al. High-resolution trace element distributions and models of trace element diffusion in enamel of Late Neolithic/Early Chalcolithic human molars from the Rioja Alavesa region (north-central Spain) help to separate biogenic from diagenetic trends. *Palaeogeogr Palaeoclimatol Palaeoecol* 2019; 532: 109260.

79. Marques MPM, Mamede AP, Vassalo AR, et al. Heat-induced Bone Diagenesis Probed by Vibrational Spectroscopy. *Sci Rep* 2018; 8: 1–13.

80. Grupe G, Hummel S. Trace element studies on experimentally cremated bone. I. Alteration of the chemical composition at high temperatures. *J Archaeol Sci* 1991; 18: 177–186.

81. Subira ME, Malgosa A. The effect of cremation on the study of trace elements. *International Journal of Osteoarchaeology* 1993; 3: 115–118.

82. Schultz JJ, Warren MW, Krigbaum JS. Analysis of human cremains: gross and chemical methods. In: Schmidt CW, Symes SA (eds) *The Analysis of Burned Human Remains*. London : Academic Press, 2008, pp. 75–94.

83. Shipman P, Foster G, Schoeninger M. Burnt bones and teeth: an experimental study of color, morphology, crystal structure and shrinkage. *J Archaeol Sci* 1984; 11: 307–325.

84. Cattaneo C, DiMartino S, Scali S, et al. Determining the human origin of fragments of burnt bone: A comparative study of histological, immunological and DNA techniques. *Forensic Sci Int* 1999; 102: 181–191.

85. Raspanti M, Guizzardi S, De Pasquale V, et al. Ultrastructure of heat-deproteinated compact bone. *Biomaterials* 1994; 15: 433–437.

86. Holden JL, Clement JG, Phakey PP. Age and temperature related changes to the ultrastructure and composition of human bone mineral. *Journal of Bone and Mineral Research* 1995; 10: 1400–1409.

87. Holden JL, Phakey PP, Clement JG. Scanning electron microscope observations of heat-treated human bone. *Forensic Science International* 1995; 74: 29–45.

88. Rogers K., Daniels P. An X-ray diffraction study of the effects of heat treatment on bone mineral microstructure. *Biomaterials* 2002; 23: 2577–2585.

89. Hiller JC, Thompson TJU, Evison MP, et al. Bone mineral change during experimental heating: An X-ray scattering investigation. *Biomaterials* 2003; 24: 5091–5097.

90. Guizzardi S, Raspanti M, Martini D, et al. Low-temperature heat-deproteinated compact bone to heal large bone defects. *Biomaterials* 1995; 16: 931–936.

91. Strydonck M Van, Boudin M, Mulder G De. The Carbon Origin of Structural Carbonate in Bone Apatite of Cremated Bones. *Radiocarbon* 2010; 52: 578–586.

92. Lebon M, Reiche I, Bahain J-J, et al. New parameters for the characterization of diagenetic alterations and heat-induced changes of fossil bone mineral using Fourier transform infrared spectrometry. *Journal of Archaeological Science* 2010; 37: 2265–2276.

93. Munro LE, Longstaffe FJ, White CD. Burning and boiling of modern deer bone: Effects on crystallinity and oxygen isotope composition of bioapatite phosphate. *Palaeogeogr Palaeoclimatol Palaeoecol* 2007; 249: 90–102.

94. Person A, Bocherens H, Mariotti A, et al. Diagenetic evolution and experimental heating of bone phosphate. *Palaeogeography, Palaeoclimatology, Palaeoecology* 1996; 126: 135–149.

95. Thompson TJU, Islam M, Bonniere M. A new statistical approach for determining the crystallinity of heat-altered bone mineral from FTIR spectra.(Report). *J Archaeol Sci* 2013; 40: 416.

96. Wang X-Y, Zuo Y, Huang D, et al. Comparative Study on Inorganic Composition and Crystallographic Properties of Cortical and Cancellous Bone. *Biomedical and Environmental Sciences* 2010; 23: 473–480.

97. Hidouri M, Dorozhkin S, Albeladi N. Thermal Behavior, Sintering and Mechanical Characterization of Multiple Ion-Substituted Hydroxyapatite Bioceramics. *J Inorg Organomet Polym Mater* 2019; 29: 87–100.

98. Raynaud S, Champion E, Bernache-Assollant D, et al. Calcium phosphate apatites with variable Ca/P atomic ratio I. Synthesis, characterisation and thermal stability of powders. *Biomaterials* 2002; 23: 1065–1072.

99. Mckinnon M, Henneberg M, Simpson E, et al. A comparison of crystal structure in fresh, burned and archaic bone – Implications for forensic sampling. *Forensic Sci Int* 2020; 313: 110328.

100. Karunadasa KS., Manoratne C., Pitawala HMTG., et al. Thermal decomposition of calcium carbonate (calcite polymorph) as examined by in-situ high-temperature X-ray powder diffraction. *J Phys Chem Solids* 2019; 134: 21–28.

101. Lee-Thorp J. Two decades of progress towards understanding fossilization processes and isotopic signals in calcified tissue minerals. *Archaeometry* 2002; 44: 435–446.

102. Mkukuma L, Skakle J, Gibson I, et al. Effect of the Proportion of Organic Material in Bone on Thermal Decomposition of Bone Mineral: An Investigation of a Variety of Bones from Different Species Using Thermogravimetric Analysis coupled to Mass Spectrometry, High-Temperature X-ray Diffraction,. *Calcified Tissue International* 2004; 75: 321–328.

103. Taylor ME, Morecroft MD, Oliver HR. The Physical Environment. *Wytham Woods*. Epub ahead of print 2011. DOI: 10.1093/acprof:osobl/9780199605187.003.0002.

104. Grupea G. Impact of the Choice of Bone Samples on Trace Element Data in Excavated Human Skeletons. *J Archaeol Sci* 1988; 15: 123–129.

105. Daniells MJ, Williams BB, Larmour RA. Excavations at Kiltierney Deerpark, County Fermanagh. *Ulster J Archaeol* 1977; 40: 32–41.

106. Trueman CN, Privat K, Field J. Why do crystallinity values fail to predict the extent of diagenetic alteration of bone mineral? *Palaeogeogr Palaeoclimatol Palaeoecol* 2008; 266: 160–167.

107. Koon HEC, Nicholson RA, Collins MJ. A practical approach to the identification of low temperature heated bone using TEM. *J Archaeol Sci* 2003; 30: 1393–1399.

108. Stathopoulou ET, Psycharis V, Chryssikos GD, et al. Bone diagenesis: New data from infrared spectroscopy and X-ray diffraction. *Palaeogeogr Palaeoclimatol Palaeoecol* 2008; 266: 168–174.

109. Pleshko N, Boskey A, Mendelsohn R. Novel infrared spectroscopic method for the

determination of crystallinity of hydroxyapatite minerals. *Biophys J* 1991; 60: 786–793.

110. Rey C, Renugopalakrishnan V, Collins B, et al. Fourier transform infrared spectroscopic study of the carbonate ions in bone mineral during aging. *Calcif Tissue Int* 1991; 49: 251–258.

111. Walters M a., Leung YC, Blumenthal NC, et al. A raman and infrared spectroscopic investigation of biological hydroxyapatite. *J Inorg Biochem* 1990; 39: 193–200.

112. Thompson TJU, Gauthier M, Islam M. The application of a new method of Fourier Transform Infrared Spectroscopy to the analysis of burned bone. *J Archaeol Sci* 2009; 36: 910–914.

113. Ellingham STD, Thompson TJU, Islam M. The Effect of Soft Tissue on Temperature Estimation from Burnt Bone Using Fourier Transform Infrared Spectroscopy. *J Forensic Sci* 2016; 61: 151–159.

114. Snoeck C, Schulting RJ, Lee-Thorp JA, et al. Impact of heating conditions on the carbon and oxygen isotope composition of calcined bone. *J Archaeol Sci* 2016; 65: 32–43.

115. Beasley MM, Bartelink EJ, Taylor L, et al. Comparison of transmission FTIR, ATR, and DRIFT spectra: Implications for assessment of bone bioapatite diagenesis. *J Archaeol Sci* 2014; 46: 16–22.

116. Ubelaker DH. Case applications of recent research on thermal effects on the skeleton. In: Thompson T (ed) *The Archaeology of Cremation: burned human remains in funerary studies*. 2015, pp. 213–227.

117. Thompson TJ., Islam M, Piduru K, et al. An investigation into the internal and external variables acting on crystallinity index using Fourier Transform Infrared Spectroscopy on unaltered and burned bone. *Palaeogeogr Palaeoclimatol Palaeoecol* 2011; 299: 168–174.

118. Piga G, Gonçalves D, Thompson TJU, et al. Understanding the Crystallinity Indices Behavior of Burned Bones and Teeth by ATR-IR and XRD in the Presence of Bioapatite Mixed with Other Phosphate and Carbonate Phases. *Int J Spectrosc* 2016; 2016: 9.

119. Grunenwald A, Keyser C, Sautereau A., et al. Revisiting carbonate quantification in apatite (bio)minerals: a validated FTIR methodology. *J Archaeol Sci*; 49: 134–141.

120. Pyle JM, Spear FS, Wark DA. Electron microprobe analysis of REE in apatite, monazite and xenotime: Protocols and pitfalls. *Rev Mineral Geochemistry* 2002; 48: 337–362.

121. Carlson WD, Donelick RA, Ketcham RA. Variability of apatite fission-track annealing kinetics: I. Experimental results. *Am Mineral* 1999; 84: 1213–1223.

122. Jochum KP, Stoll B, Herwig K, et al. MPI-DING reference glasses for in situ microanalysis: New reference values for element concentrations and isotope ratios. *Geochemistry, Geophys Geosystems* 2006; 7: n/a-n/a.

123. Goodman D. Encyclopedia of Analytical Chemistry: Applications, Theory, and Instrumentation. *CHOICE Curr Rev Acad Libr* 2001; 39: 287.

124. Holcomb DW, Younger RA. Thermal decomposition of human tooth enamel. *Calcif Tissue Int* 1980; 31: 198–201.

125. Praprotnik M, Janežič D. Molecular dynamics integration and molecular vibrational theory. III. The infrared spectrum of water. *J Chem Phys* 2005; 17: 174102.

126. Gerakines PA, Schutte WA, Greenberg JM, et al. The infrared band strengths of H2O, CO and CO2 in laboratory simulations of astrophysical ice mixtures. *Astron Astrophys* 1995; 296: 810–818.

127. Dowker SEP, Elliott JC. Infrared adsorption bands from NCO- and NCN2- in heated

carbonate-containing apatites prepared in the presence of NH4 + ions. *Calcif Tissue Int* 1979; 29: 177–178.

128. LeGeros RZ, Trautz OR, Klein E, et al. Two types of carbonate substitution in the apatite structure. *Experientia* 1969; 25: 5–7.

129. LeGeros RZ, LeGeros JP. Carbonate analyses of synthetic, mineral and biological apatites. *J Dent Res* 1983; 82: 259.

130. Thompson TJU, Inglis J. Differentiation of serrated and non-serrated blades from stab marks in bone. *Int J Legal Med* 2009; 123: 129–135.

131. Rey C, Collins B, Goehl T, et al. The carbonate environment in bone mineral: a resolution-enhanced Fourier transform infrared spectroscopy study. *Calcif Tissue Int* 1989; 45: 157–164.

132. Mamede AP, Gonçalves D, Marques MPM, et al. Burned bones tell their own stories: A review of methodological approaches to assess heat-induced diagenesis. *Appl Spectrosc Rev* 2018; 53: 603–635.

133. Kloprogge JT, Hickey L, Frost RL. FT-Raman and FT-IR spectroscopic study of synthetic Mg/Zn/Al-hydrotalcites. *J Raman Spectrosc*; 35: 967–974.

134. Miller LM, Vairavamurthy V, Chance MR, et al. In situ analysis of mineral content and crystallinity in bone using infrared micro-spectroscopy of the ν 4 PO 43− vibration. *Biochim Biophys acta Gen Subj* 2001; 1527: 11–19.

135. Keenan SW, Engel AS. Early diagenesis and recrystallization of bone. *Geochim Cosmochim Acta* 2017; 196: 209–223.

136. Piga G, Thompson TJU, Malgosa A, et al. The potential of X-ray diffraction in the analysis of burned remains from forensic contexts. *J Forensic Sci* 2009; 54: 534–539.

137. Beckett S. *Inter-species variation in bone mineral*. Cranfield University, 2009.

138. Greenwood C, Rogers K, Beckett S, et al. Initial observations of dynamically heated bone. *Cryst Res Technol* 2013; 48: 1073–1082.

139. Danilchenko SN, Kalinkevich AN, Moskalenko RA, et al. Structural and crystal-chemical characteristics of the apatite deposits from human aortic walls. *Interv Med Appl Sci* 2018; 10: 110–119.

140. Bushinsky DA, Gavrilov KL, Chabala JM, et al. Contribution of Organic Material to the Ion Composition of Bone. *J bone Miner Res* 2000; 15: 2026–2032.

141. Gallo G, Fyhrie M, Paine C, et al. Characterization of structural changes in modern and archaeological burnt bone: Implications for differential preservation bias. *PLoS One* 2021; 16: e0254529–e0254529.

142. Yoo DS, Cho JS, Chung Y-C, et al. Defect structures of sodium and chloride co-substituted hydroxyapatite and its osseointegration capacity. *J Mater Sci* 2021; 56: 5493–5508.

143. Beckett S, Rogers KD, Clement JG. Inter-species variation in bone mineral behavior upon heating. *J Forensic Sci* 2011; 56: 571–579.

144. Lambert JB, Vlasak S, Simpson, et al. Bone diagenesis and dietary analysis. *J Hum Evol* 1985; 14: 477–482.

145. Parker RB, Toots H, Murphy J. Leaching of sodium from skeletal parts during fossilization. *Geochim Cosmochim Acta* 1974; 38: 1317–1321.

146. Maiti GC, Freund F. Incorporation of chlorine into hydroxy-apatite. *J Inorg Nucl Chem* 1981;

43: 2633–2637.

147. Scharlotta I, Goriunova OI, Weber A. Micro-sampling of human bones for mobility studies: diagenetic impacts and potentials for elemental and isotopic research. *J Archaeol Sci* 2013; 40: 4509–4527.

Figure Captions

Figure 1. – The FTIR spectra of the means of each PMI group before (upper image) and after (lower image) burning. Labelled are the peak assignments of interest

Figure 2. – Loadings of the principal component analysis

Figure 3. – Average elemental concentration (wt %) of the experimental bones using the EMPA data. Mean ± 2 standard errors for each measured element as a function of time in unburnt and burnt bone.

Figure 4. – Average elemental concentration (wt %) of the Neolithic cremated human remains for each zone. Mean ± 2 standard errors for each measured major and trace element in archaeological cremated bone. The backscattered electron microscopy (BSEM) image represents an example of a bone cross section.

Figure 5. – Potassium wt% content in experimental unburnt (upper) and burnt (lower) bone by zone.

Figure 6. – Linear discriminant analysis (LDA) on the EMPA dataset. A: Separation of unburnt and burnt bone by LDA. Contributions: 'Al2O3': 0.244, 'CaO': -6.882,'Cl': 3.216,'FeO': 0.07,'K2O': 0.607,'MgO':- 1.036,'MnO': -0.056, 'Na2O': -0.545,'P2O5': -3.97,'SiO2': -0.902,'SrO': 0.199, 'Total': 13.08. B: Clusters created by LDA of the unburnt (left) and burnt (right) PMI groups.

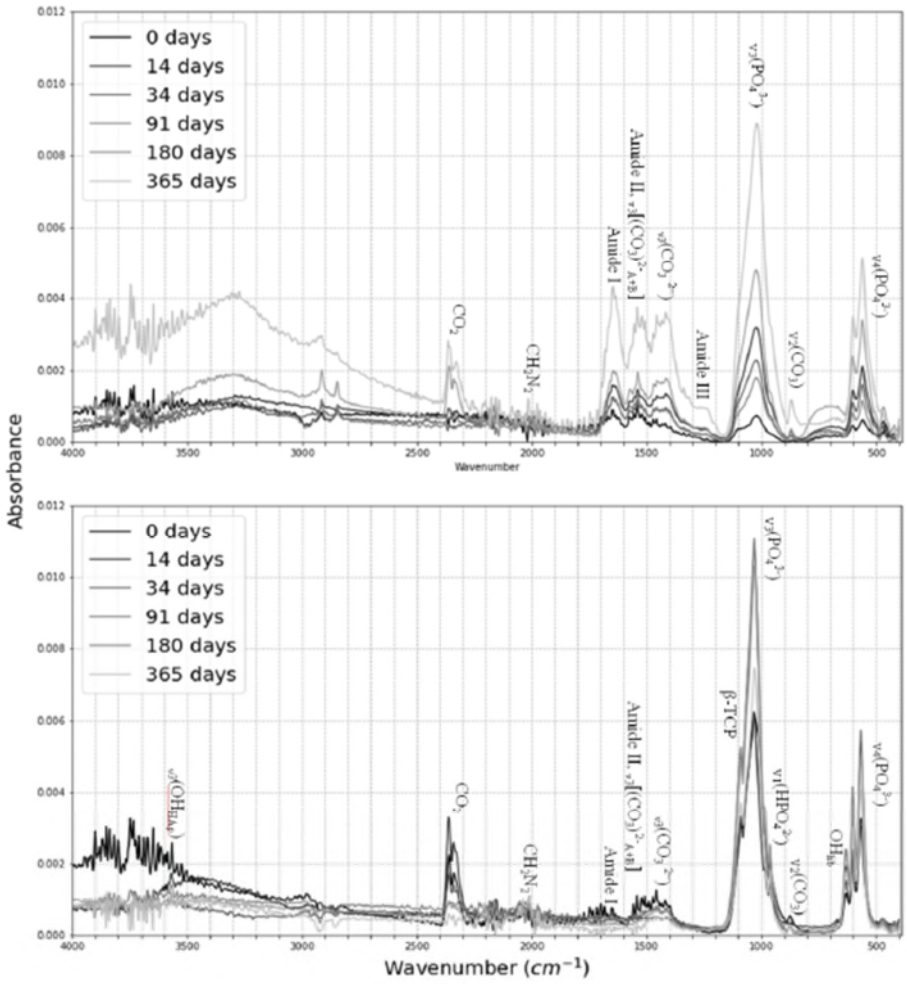

Fig. 1 - The FTIR spectra of the means of each PMI group before (upper image) and after (lower image) burning. Labelled are the peak assignments of interest.

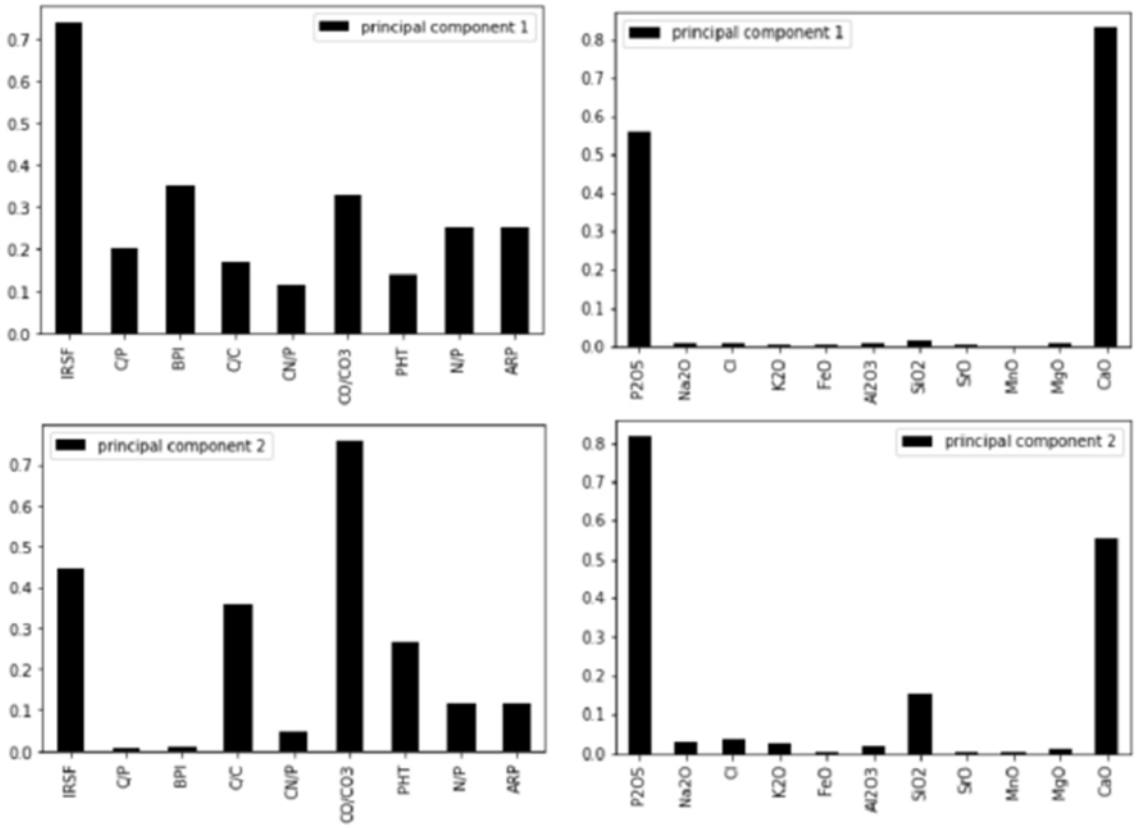

Fig. 2 – Loadings of the principal component analysis.

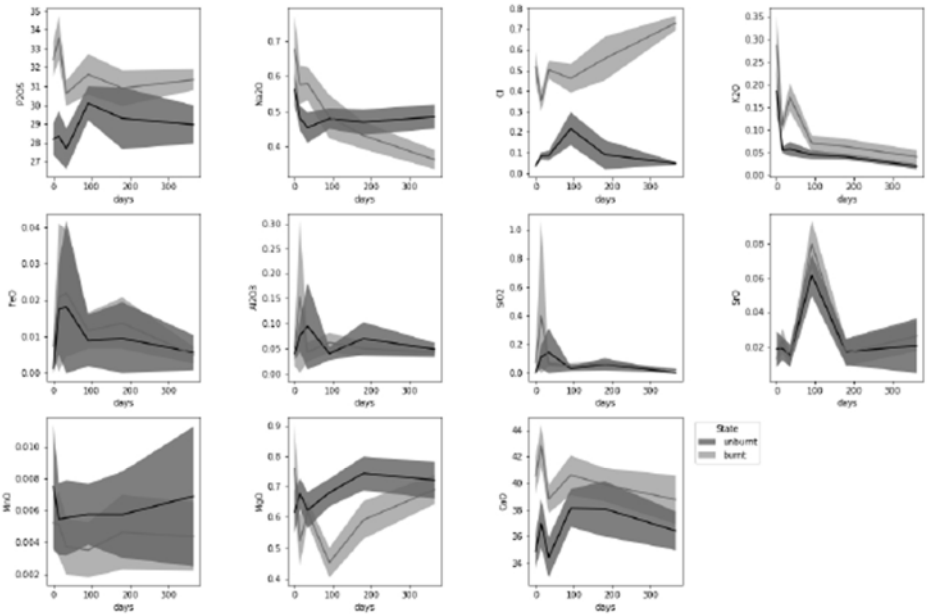

Fig. 3 – Average elemental concentration (wt %) of the experimental bones using the EMPA data. Mean ± 2 standard errors for each measured element as a function of time in unburnt and burnt bone.

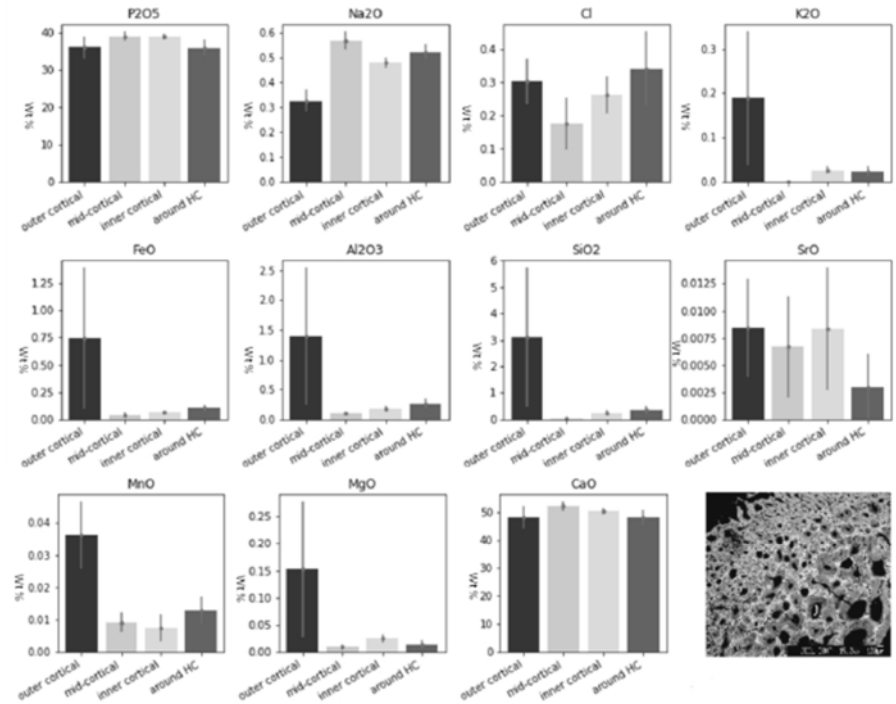

Fig. 4 – Average elemental concentration (wt %) of the Neolithic cremated human remains for each zone. Mean ± 2 standard errors for each measured major and trace element in archaeological cremated bone. The backscattered electron microscopy (BSEM) image represents an example of a bone cross section.

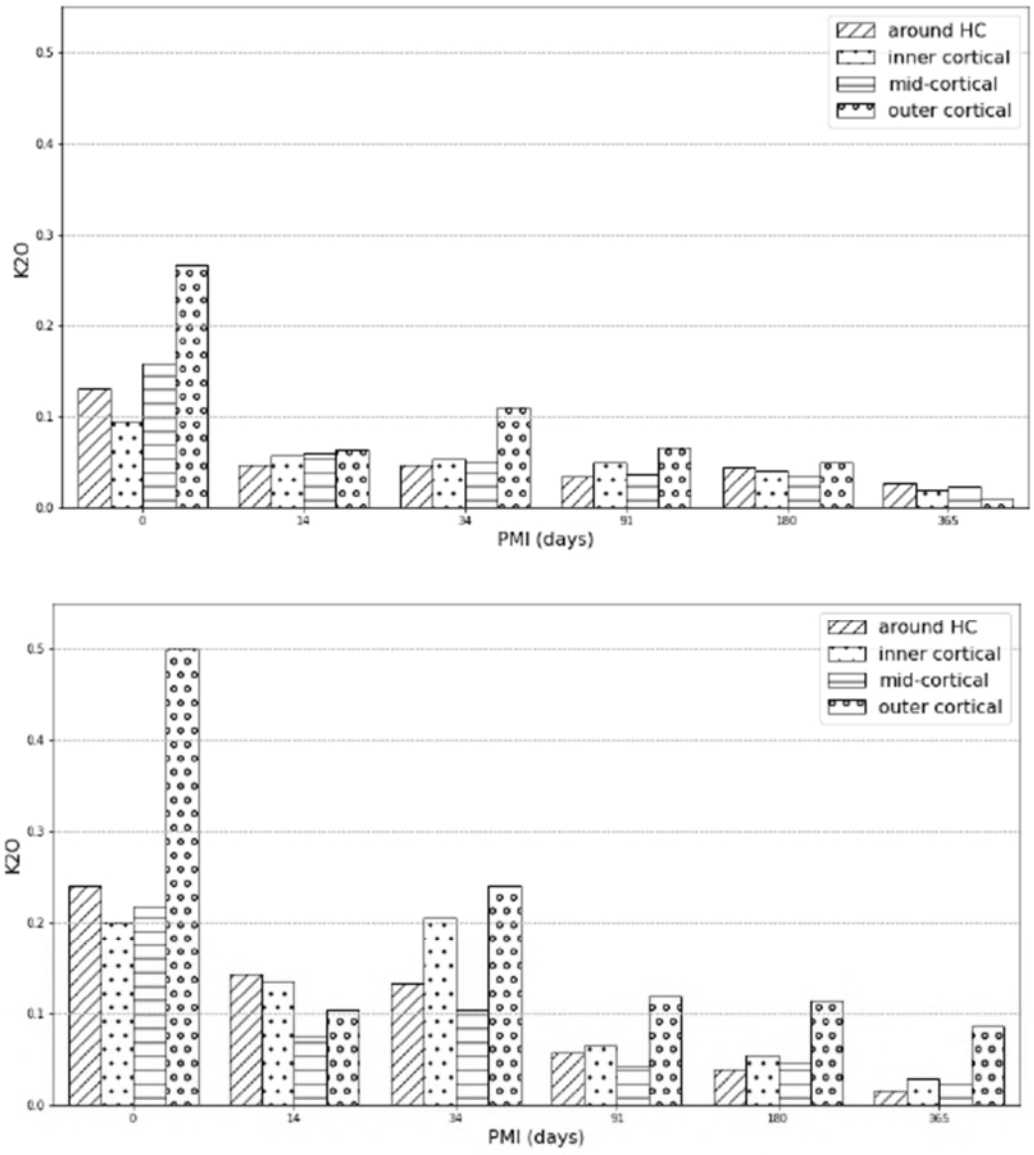

Fig. 5 – Potassium wt% content in experimental unburnt (upper) and burnt (lower) bone by zone.

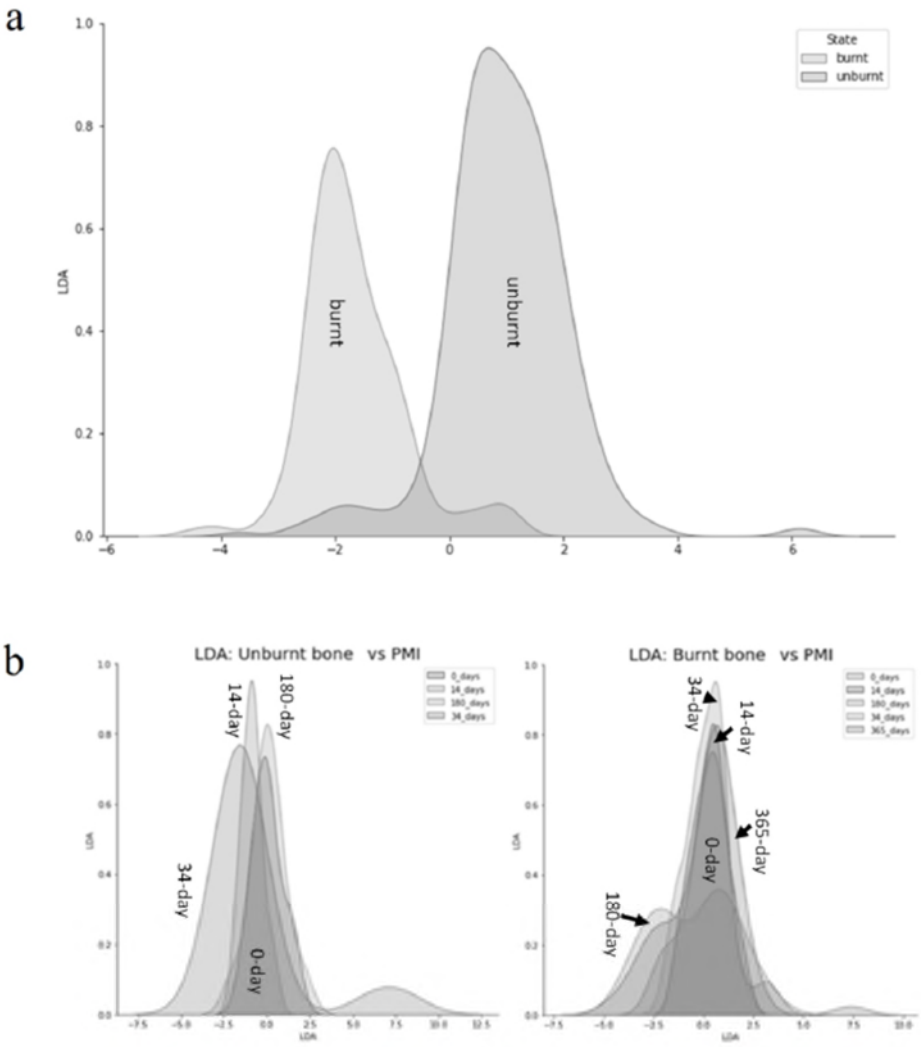

Fig. 6 – Linear discriminant analysis (LDA) on the EMPA dataset. A: Separation of unburnt and burnt bone by LDA. Contributions: 'Al2O3': 0.244, 'CaO': -6.882,'Cl': 3.216,'FeO': 0.07,'K2O': 0.607,'MgO':-1.036,'MnO': -0.056, 'Na2O': -0.545,'P2O5': -3.97,'SiO2': -0.902,'SrO': 0.199, 'Total': 13.08. B: Clusters created by LDA of the unburnt (left) and burnt (right) PMI groups.

Supplementary Material

Component	Bone (wt%)
Ca	36.6
P	17.1
CO_2	4.8
Na	1
K	0.07
Mg	0.6
Sr	0.05
Cl	0.1
F	0.1
Ca/P molar	1.65

Suppl. 1 - The reported elemental concentration of bone ±1% variability due to diet, age, and anatomical variation (after Elliott 2002, 430).

Heat-Induced Elemental Changes in Bioapatite			
Element(s)	**Noted Differences**	**Notes**	**Citations**
Sr, Mg, Zn, Cu, Ba, V, Mn, Pb	Lower in archaeological calcined bones than in unburnt bones.	Potential contamination from the soil in unburnt bones.	63
Sr	Stable	Calcined bones do not exhibit uptake or loss of Sr, making them a reliable substrate for strontium isotope analysis.	114
Ca	Increase	Not statistically significant	81
	Stable	Together with P	43
	Decrease	Different between temperature groups, but not between archaeological and modern bones.	99
Mg, F	Decrease	At >500°C and only in specific surface zones	97
Fe	Increase	Uptake in archaeological charred enamel suggested to be caused by pores and fissures from burning.	78

Suppl. 2. -- Documented differences in elemental concentration due to burning in bone in the literature.

Wavenumber (cm^{-1})	Notation	Assignment	Information retrieved
(565 + 603)/595	IRSF	Crystallinity Index or Splitting Factor, splitting between the $_{v3}PO_4$ domain	Reveals the structural order of the crystals of the inorganic portion of bones [4,7,93,107,129,148,149]
1660/1035	APR	Amide to phosphate ratio	Collagen to phosphate ratio[150]
1415/1035	C/P	Carbonate (CO_3) to phosphate (P) ratio	Type B carbonate content of the sample [112]
1415/603	BPI	Type B carbonate to phosphate ratio	Amount of type B carbonate
1540/603	API	Type A carbonate to Phosphate	Amount of type A carbonate (only calculated from burnt bone due to overlap with amide II)
1450/1415	C/C	type B to type A carbonate	Amount of type B carbonate compared to type A carbonate
2010/1035	CN/P	Cyanamide (CN_2^{2-}) to phosphate	Cyanamide presence[8]
1650/1415	CO/CO3	Carbonyl to Carbonate ratio	Organic to mineral ratio
625/610	PHT	Phosphate high temperature	Bones burnt $>700^0C$[95]
1660/1035	N/P	Amide I to Phosphate	Organic to mineral ratio

Suppl. 3. - Measured IR ratios and their assignments from the literature.

Descriptive Statistics of the IRSF Measurements

PMI (days)	Sample	Unburnt	Burnt	Mean Unburnt	Mean Burnt	Mean % increase	Std Unburnt	Std burnt	CV unburnt	CV burnt
0	WSFresh	3.16	5.16	3.08	5.03	52.42	0.44	0.19	0.13	0.04
	SWF2FR3	2.99	5.04							
	SWF2FR4	N/A	4.93							
	WS4_FR	N/A	5.24							
	WS5_FR	N/A	4.76							
14	WSF2D2W1	2.49	3.58	2.88	4.10	42.36	0.23	0.75	0.08	0.18
	WSF2D2W2	2.91	5.08							
	WSF2D2W3	3.06	3.2							
	WSF2D2W4	3.01	4.56							
	WSF2D2W5	2.95	4.07							
34	WSF3D1M1	3.18	4.71	3.23	4.45	37.77	0.21	0.27	0.06	0.06
	WSF3D1M2	3.53	4.29							
	WSF3D1M3	2.98	4.68							

	WSF3D1M4	3.31	4.06							
	WSF3D1M5	3.14	4.49							
91	WSF3D3M1	3.48	5.04	3.31	5.19	57.27	0.12	0.37	0.03	0.07
	WSF3D3M2	3.28	5.57							
	WSF3D3M3	3.22	5.41							
	WSF3D3M4	3.25	4.75							
180	WSF5D6M1	2.96	5.26	3.07	4.77	0.55	0.07	0.34	0.03	0.07
	WSF5D6M2	3.03	4.36							
	WSF5D6M3	3.16	4.55							
	WSF5D6M4	3.12	4.83							
	WSF5D6M5	3.1	4.85							
365	SWF5D1Y1	5.04	4.77	5.04	4.77	-5.35	0.00	0.00	0.00	0.00

Suppl. 4 - The mean IRSF values for the unburnt and burnt groups at different PMIs.

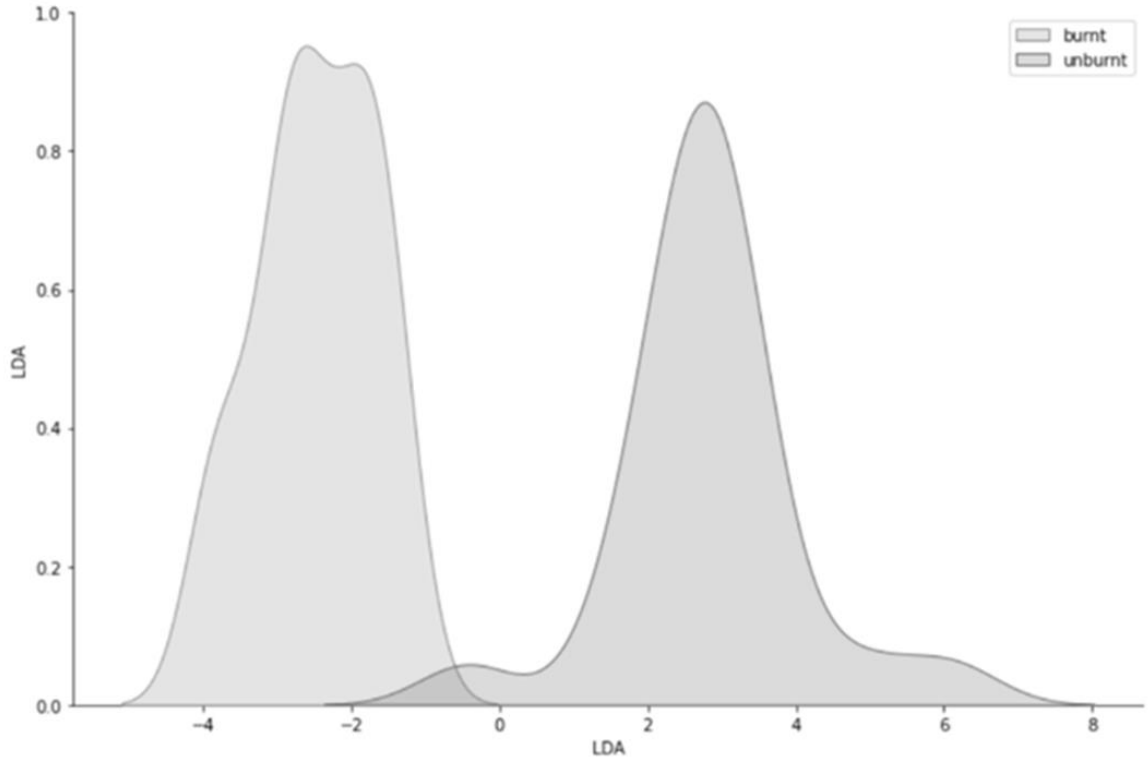

Suppl. 5 -- Linear Discriminant Analysis (LDA) on the FTIR dataset to discriminate between states (unburnt vs burnt) bone. Contributions: 'ARP': -3.806, 'BPI': 3.204, 'C/C': -3.97, 'C/P': -21.982, 'CN/P': 14.449, 'CO/CO3': -1.345, 'IRSF': 4.651, 'N/P': -3.806, 'PHT': 19.552.

PMI	State	Zone	N	**P2O5**		**Na2O**		**Cl**		**K2O**		**FeO**		**Al2O3**		**SiO2**		**SrO**		**MnO**		**MgO**		**CaO**	
				mean	CV	mean	CV	mean	CV	mean	CV	mean	CV	mean	CV	mean	CV	mean	CV	mean	CV	mean	CV	mean	CV
0 days	U	HC	3	27.87	0.07	0.51	0.18	0.03	0.00	0.13	0.00	0.00	0.00	0.03	1.00	0.00	0.00	0.02	1.00	0.01	1.00	0.56	0.16	33.81	0.09
		IC	2	27.24	0.02	0.46	0.02	0.04	0.00	0.10	0.10	0.00	0.00	0.05	0.20	0.00	0.00	0.00	0.00	0.01	1.00	0.54	0.20	34.03	0.04
		MC	5	29.34	0.05	0.57	0.11	0.03	0.33	0.16	0.50	0.00	0.00	0.05	0.40	0.01	3.00	0.02	1.00	B.D.	0.00	0.68	0.16	37.31	0.05
		OC	6	27.69	0.06	0.62	0.16	0.04	0.25	0.27	0.44	B.D.	0.00	0.04	0.75	0.00	0.00	0.02	1.00	B.D.	0.00	0.62	0.31	33.67	0.06
		Total	16	**28.03**	0.05	**0.54**	0.11	**0.03**	0.33	**0.16**	0.31	**0.00**	0.00	**0.04**	0.50	**0.00**	0.00	**0.02**	1.00	**0.01**	1.00	**0.60**	0.20	**34.70**	0.06
	B	HC	14	32.44	0.12	0.86	0.65	0.35	0.46	0.24	0.75	B.D.	0.00	0.10	3.20	0.08	0.88	0.01	2.00	B.D.	0.00	0.75	0.71	41.34	0.12
		IC	22	32.79	0.16	0.57	0.40	0.56	0.80	0.20	0.55	B.D.	0.00	0.04	2.25	0.06	0.83	0.01	2.00	B.D.	0.00	0.85	1.20	42.07	0.17
		MC	18	32.15	0.06	0.58	0.41	0.51	0.33	0.22	0.50	B.D.	0.00	0.02	1.50	0.09	1.33	0.02	1.00	B.D.	0.00	0.59	0.17	40.40	0.05
		OC	18	32.28	0.11	0.77	0.66	0.60	0.47	0.50	0.90	B.D.	0.00	0.05	0.80	0.07	1.00	B.D.	0.00	B.D.	0.00	0.82	0.13	38.20	0.18
		Total	72	**32.42**	0.11	**0.69**	0.55	**0.51**	0.51	**0.29**	0.72	**N/A**	0.00	**0.05**	2.40	**0.08**	1.00	**0.01**	2.00	**N/A**	0.00	**0.75**	0.59	**40.50**	0.13
14 days	U	HC	12	29.49	0.12	0.46	0.13	0.08	0.75	0.05	0.40	B.D.	0.00	0.05	1.20	0.02	1.50	0.02	1.50	B.D.	0.00	0.72	0.18	38.31	0.11
		IC	16	28.18	0.08	0.47	0.34	0.09	0.67	0.06	0.33	0.02	3.00	0.10	1.40	0.08	1.63	0.01	3.00	B.D.	0.00	0.63	0.29	36.94	0.11
		MC	18	30.95	0.10	0.56	0.13	0.05	0.40	0.06	0.50	B.D.	0.00	0.03	1.33	0.02	1.50	0.03	0.67	B.D.	0.00	0.78	0.12	40.35	0.12
		OC	7	20.16	0.32	0.33	0.33	0.14	0.93	0.06	0.50	0.08	0.75	0.16	1.25	0.59	1.14	B.D.	0.00	B.D.	0.00	0.45	0.47	26.11	0.31
		Total	53	**27.19**	0.14	**0.46**	0.22	**0.09**	0.78	**0.06**	0.50	**0.05**	0.60	**0.09**	1.22	**0.18**	1.17	**0.02**	1.00	**N/A**	0.00	**0.65**	0.23	**35.43**	0.15
	B	HC	15	31.78	0.19	0.62	0.53	0.33	0.48	0.14	0.64	0.06	3.00	0.58	2.28	1.67	3.60	0.02	1.50	B.D.	0.00	0.61	0.85	40.83	0.17
		IC	17	35.60	0.13	0.56	0.30	0.33	0.82	0.13	0.54	0.01	2.00	0.04	0.50	0.06	1.17	0.03	1.00	B.D.	0.00	0.53	0.53	45.66	0.15
		MC	21	34.41	0.13	0.57	0.42	0.30	0.57	0.08	0.50	B.D.	0.00	0.03	1.00	0.02	1.50	0.02	1.00	B.D.	0.00	0.43	0.74	44.37	0.13
		OC	17	32.15	0.11	0.55	0.31	0.46	0.43	0.10	0.50	0.02	1.50	0.03	1.00	0.09	1.00	0.02	1.50	B.D.	0.00	0.56	0.36	39.77	0.14
		Total	70	**33.49**	0.14	**0.58**	0.40	**0.35**	0.57	**0.11**	0.55	**0.03**	2.00	**0.17**	2.06	**0.46**	3.37	**0.02**	1.50	**N/A**	0.00	**0.53**	0.62	**42.66**	0.15

34 days	U	HC	10	28.75	0.08	0.49	0.27	0.08	0.38	0.05	0.60	B.D.	0.00	0.04	0.75	0.05	1.00	0.02	1.00	B.D.	0.00	0.71	0.15	36.61	0.10
		IC	11	26.76	0.12	0.43	0.42	0.08	0.38	0.05	0.60	B.D.	0.00	0.07	0.57	0.14	1.14	0.01	2.00	B.D.	0.00	0.52	0.46	32.67	0.12
		MC	12	28.53	0.09	0.47	0.15	0.07	0.43	0.05	0.40	B.D.	0.00	0.05	1.00	0.02	2.00	0.01	2.00	B.D.	0.00	0.69	0.16	35.43	0.11
		OC	5	25.41	0.23	0.41	0.37	0.17	1.00	0.11	1.00	0.11	1.73	0.38	1.89	0.65	2.17	0.02	1.50	0.01	0.00	0.53	0.32	31.48	0.24
		Total	38	**27.36**	0.13	**0.45**	0.29	**0.10**	0.60	**0.07**	0.71	**0.11**	0.45	**0.13**	1.62	**0.22**	1.86	**0.02**	1.00	**0.01**	1.00	**0.61**	0.26	**34.05**	0.14
	B	HC	13	30.65	0.12	0.58	0.22	0.47	0.40	0.13	0.77	B.D.	0.00	0.07	1.86	0.06	1.00	0.01	2.00	B.D.	0.00	0.62	0.29	39.13	0.14
		IC	16	30.95	0.11	0.62	0.42	0.51	0.20	0.20	0.75	B.D.	0.00	0.03	1.33	0.06	0.83	0.02	1.00	B.D.	0.00	0.59	0.27	38.99	0.12
		MC	17	31.18	0.04	0.53	0.26	0.45	0.38	0.10	0.30	B.D.	0.00	0.04	1.50	0.05	1.00	0.01	2.00	B.D.	0.00	0.59	0.20	39.91	0.04
		OC	17	29.74	0.07	0.59	0.32	0.58	0.36	0.24	0.54	0.06	0.00	0.04	1.25	0.09	1.00	0.01	2.00	B.D.	0.00	0.67	0.15	37.20	0.11
		Total	63	**30.63**	0.08	**0.58**	0.31	**0.50**	0.34	**0.17**	0.59	**0.06**	0.67	**0.04**	1.75	**0.06**	1.00	**0.01**	2.00	**N/A**	0.00	**0.62**	0.23	**38.81**	0.10
91 days	U	HC	11	31.17	0.06	0.48	0.23	0.22	1.36	0.03	0.67	B.D.	0.00	0.03	1.33	0.02	1.50	0.06	0.83	B.D.	0.00	0.77	0.09	38.97	0.11
		IC	10	30.65	0.09	0.46	0.17	0.25	1.16	0.05	0.60	B.D.	0.00	0.03	1.33	B.D.	0.00	0.07	0.57	B.D.	0.00	0.57	0.21	39.56	0.10
		MC	15	30.49	0.11	0.54	0.17	0.16	1.38	0.04	0.50	B.D.	0.00	0.03	1.00	0.03	1.67	0.06	0.50	B.D.	0.00	0.76	0.08	39.12	0.14
		OC	11	27.93	0.12	0.41	0.20	0.27	1.26	0.07	0.71	0.03	1.67	0.07	1.00	0.07	1.29	0.06	0.83	B.D.	0.00	0.57	0.37	34.60	0.11
		Total	47	**30.06**	0.09	**0.47**	0.19	**0.22**	1.27	**0.05**	0.60	**0.03**	0.67	**0.04**	1.00	**0.04**	1.25	**0.06**	0.67	**N/A**	0.00	**0.67**	0.18	**38.06**	0.12
	B	HC	16	29.89	0.20	0.57	0.61	0.44	0.64	0.06	0.33	0.02	1.50	0.12	1.17	0.07	1.14	0.07	0.71	B.D.	0.00	0.46	0.41	38.10	0.20
		IC	17	31.89	0.07	0.58	0.48	0.49	0.51	0.06	0.33	B.D.	0.00	0.05	0.80	0.06	1.00	0.08	0.63	B.D.	0.00	0.45	0.40	40.53	0.09
		MC	17	34.22	0.13	0.48	0.23	0.34	0.85	0.04	0.50	B.D.	0.00	0.03	0.67	0.04	1.25	0.08	0.75	B.D.	0.00	0.42	0.60	44.29	0.15
		OC	18	30.51	0.11	0.32	0.38	0.56	0.54	0.12	1.00	0.01	2.00	0.06	0.83	0.04	2.00	0.08	0.75	B.D.	0.00	0.47	0.40	39.37	0.12
		Total	68	**31.63**	0.13	**0.49**	0.45	**0.46**	0.61	**0.07**	0.71	**0.01**	2.00	**0.06**	1.00	**0.05**	1.40	**0.08**	0.75	**N/A**	0.00	**0.45**	0.44	**40.57**	0.14
180 days	U	HC	8	27.44	0.33	0.42	0.36	0.22	2.14	0.04	0.50	B.D.	0.00	0.08	1.13	0.02	1.50	0.02	1.50	B.D.	0.00	0.70	0.34	34.39	0.30
		IC	6	30.77	0.12	0.49	0.10	0.05	0.60	0.04	0.50	B.D.	0.00	0.05	0.60	0.06	1.00	B.D.	0.00	B.D.	0.00	0.67	0.16	39.14	0.13
		MC	14	29.98	0.09	0.53	0.11	0.06	0.50	0.03	0.33	B.D.	0.00	0.04	0.75	0.03	1.00	B.D.	0.00	B.D.	0.00	0.81	0.11	39.87	0.10

		OC	10	28.94	0.16	0.41	0.29	0.05	0.40	0.05	0.60	0.03	2.00	0.12	1.42	0.14	1.71	0.03	0.67	0.01	1.00	0.73	0.30	37.79	0.15
		Total	38	**29.28**	0.17	**0.46**	0.20	**0.10**	1.40	**0.04**	0.50	**0.03**	0.67	**0.07**	1.14	**0.06**	1.50	**0.03**	0.67	**0.01**	1.00	**0.73**	0.22	**37.80**	0.16
	B	HC	8	31.09	0.13	0.38	0.32	0.33	1.03	0.04	0.25	0.01	3.00	0.06	1.17	0.08	0.88	0.02	1.00	B.D.	0.00	0.67	0.24	39.43	0.16
		IC	11	28.86	0.12	0.38	0.26	0.73	0.59	0.05	0.40	0.03	1.00	0.04	0.75	0.09	1.00	0.02	1.50	B.D.	0.00	0.57	0.33	37.42	0.11
		MC	12	31.22	0.06	0.48	0.13	0.49	0.53	0.05	0.20	B.D.	0.00	0.03	1.33	0.02	2.00	0.01	3.00	B.D.	0.00	0.58	0.31	41.40	0.04
		OC	10	32.61	0.04	0.47	0.38	0.64	0.31	0.11	0.82	B.D.	0.00	0.07	0.57	0.07	1.00	0.01	2.00	B.D.	0.00	0.57	0.46	41.07	0.05
		Total	41	**30.94**	0.09	**0.43**	0.26	**0.54**	0.57	**0.06**	0.67	**0.02**	1.00	**0.05**	1.00	**0.07**	1.00	**0.02**	1.00	**N/A**	0.00	**0.60**	0.33	**39.83**	0.09
365 days	U	HC	3	29.45	0.05	0.53	0.21	0.03	0.33	0.03	0.67	0.00	0.00	0.07	0.43	0.02	1.50	0.03	1.00	0.02	0.50	0.76	0.01	37.22	0.05
		IC	7	27.89	0.08	0.48	0.13	0.06	0.17	0.02	0.50	B.D.	0.00	0.04	0.50	0.00	0.00	0.02	2.00	B.D.	0.00	0.69	0.16	34.53	0.09
		MC	4	30.25	0.05	0.49	0.10	0.04	0.25	0.02	0.50	B.D.	0.00	0.03	0.67	0.00	0.00	0.01	3.00	B.D.	0.00	0.75	0.17	38.12	0.05
		OC	2	29.41	0.08	0.43	0.12	0.04	0.00	0.01	0.00	0.02	1.00	0.07	0.14	0.00	0.00	0.03	1.33	0.01	1.00	0.70	0.43	38.43	0.03
		Total	16	**29.25**	0.06	**0.48**	0.15	**0.04**	0.25	**0.02**	0.50	**0.01**	1.00	**0.05**	0.40	**0.00**	0.00	**0.02**	1.50	**0.01**	1.00	**0.73**	0.18	**37.07**	0.05
	B	HC	11	30.65	0.08	0.30	0.27	0.76	0.22	0.02	0.50	B.D.	0.00	0.05	1.00	0.03	1.00	0.02	1.50	B.D.	0.00	0.76	0.18	38.30	0.07
		IC	11	30.64	0.05	0.35	0.17	0.80	0.09	0.03	0.67	B.D.	0.00	0.05	0.80	0.02	1.50	0.02	1.50	B.D.	0.00	0.51	0.18	37.87	0.05
		MC	12	32.08	0.03	0.45	0.20	0.64	0.17	0.02	1.00	B.D.	0.00	0.04	0.75	0.02	1.50	0.04	0.75	B.D.	0.00	0.70	0.16	38.03	0.32
		OC	14	31.81	0.07	0.35	0.23	0.73	0.12	0.09	0.78	B.D.	0.00	0.03	0.67	0.03	1.00	0.02	1.50	B.D.	0.00	0.77	0.22	40.41	0.07
		Total	48	**31.30**	0.06	**0.36**	0.22	**0.73**	0.15	**0.04**	0.75	**N/A**	0.00	**0.04**	1.00	**0.02**	1.50	**0.03**	1.00	**N/A**	0.00	**0.68**	0.19	**38.65**	0.12
Neol.	B	HC	10	35.92	0.19	0.52	0.19	0.34	1.03	0.02	2.00	0.10	0.90	0.26	1.12	0.35	1.37	0.00	1.38	0.01	1.00	0.01	2.00	48.11	0.18
		IC	12	38.98	0.08	0.48	0.15	0.26	0.77	0.03	1.00	0.06	0.00	0.18	0.78	0.24	1.50	0.01	1.49	B.D.	0.00	0.03	1.00	50.54	0.07
		MC	12	39.13	0.12	0.57	0.23	0.17	1.59	B.D.	N/A	0.04	2.00	0.10	0.70	0.04	1.50	0.01	1.30	B.D.	0.00	B.D.	0.00	52.13	0.11
		OC	13	36.15	0.29	0.33	0.48	0.30	0.83	0.19	2.84	0.74	0.00	1.39	2.97	3.09	3.08	0.01	3.08	0.04	1.00	0.15	3.00	48.22	0.29
		Total	47	**37.54**	0.17	**0.47**	0.23	**0.27**	1.00	**0.08**	1.88	**0.24**	0.00	**0.48**	2.42	**0.93**	2.80	0.01	1.81	**0.02**	1.00	**0.06**	2.17	**49.75**	0.16

Suppl. 6. - Mean major and trace elements chemistry , coefficient of variation (CV) of the unburnt (U) and burnt (B) bone samples with different PMIs. N= analysis per specimen.